# Control Optimization

Dehaeze Thomas

April 8, 2025

# Contents


**1 Multiple Sensor Control** **4**
- 1.1 Sensor fusion - Introduction . . . 6
- 1.2 Sensor Fusion and Complementary Filters Requirements . . . 7
- 1.3 Complementary Filters Shaping . . . 11
- 1.4 Synthesis of a set of three complementary filters . . . 14

**2 Decoupling** **18**
- 2.1 Test Model . . . 19
- 2.2 Control in the frame of the struts . . . 20
- 2.3 Jacobian Decoupling . . . 22
- 2.4 Modal Decoupling . . . 25
- 2.5 SVD Decoupling . . . 27
- 2.6 Comparison of decoupling strategies . . . 30

**3 Closed-Loop Shaping using Complementary Filters** **33**
- 3.1 Control Architecture . . . 34
- 3.2 Translating the performance requirements into the shapes of the complementary filters . 36
- 3.3 Complementary filter design . . . 40
- 3.4 Numerical Example . . . 41

**Bibliography** **47**

When controlling a MIMO system (specifically parallel manipulator such as the Stewart platform?)

- ☐ **Should the quick review of Stewart platform control be here?** In that case it should be possible to highlight three areas:
  - use of multiple sensors
  - decoupling strategy
  - control optimization

Several considerations:

- Section 1: How to most effectively use/combine multiple sensors
- Section 2: How to decouple a system
- Section 3: How to design the controller

# 1 Multiple Sensor Control

As was shown during the literature review of Stewart platforms, there is a large diversity of designs and included sensors and actuators. Depending on the control objectives, which may include active damping, vibration isolation, or precise positioning, different sensor configurations are implemented. The specific selection of the sensors, whether inertial sensors, force sensors, or relative position sensors, is heavily influenced by the control requirements of the system.

In cases where multiple control objectives must be achieved simultaneously, as is the case for the Nano Active Stabilization System (NASS) where the Stewart platform must both position the sample and provide isolation from micro-station vibrations, combining multiple sensors within the control architecture has been demonstrated to yield significant performance benefits. From the literature, three principal approaches for combining sensors have been identified: High Authority Control-Low Authority Control (HAC-LAC), sensor fusion, and two-sensor control architectures.

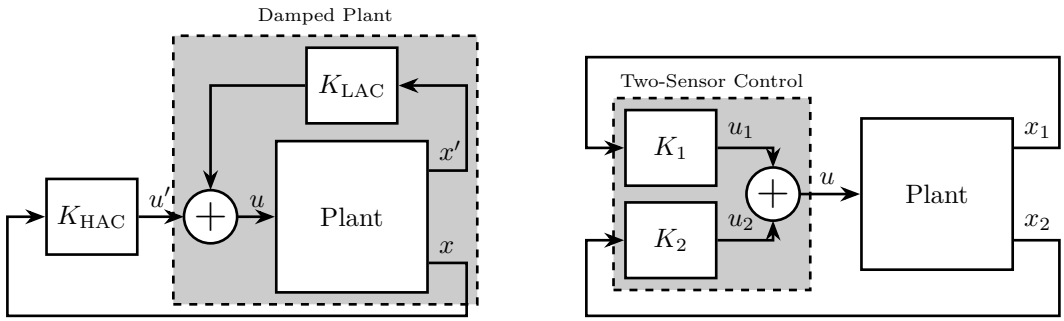


**(a)** HAC LAC




**(b)** Two Sensor Control

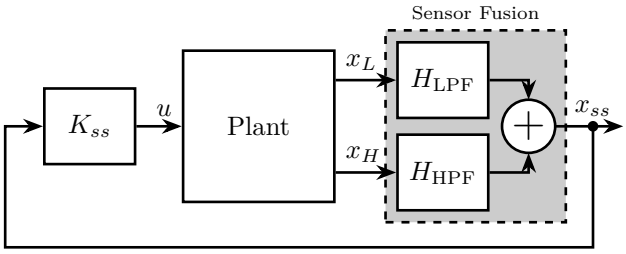


**(c)** Sensor Fusion

**Figure 1.1:** Different control strategies when using multiple sensors. High Authority Control / Low Authority Control (a). Sensor Fusion (c). Two-Sensor Control (b)

The HAC-LAC approach, used during the conceptual phase, represents a dual-loop control strategy where two control loops utilize different sensors for different purposes (Figure 1.1a). In [4], vibration isolation is provided by accelerometers collocated with the voice coil actuators, while external rotational

sensors are utilized to achieve pointing control. In [1], force sensors collocated with the magnetostrictive actuators are used for active damping using decentralized IFF, and subsequently accelerometers are employed for adaptive vibration isolation. Similarly, in [3], piezoelectric actuators with collocated force sensors are used in a decentralized manner to provide active damping while accelerometers are implemented in an adaptive feedback loop to suppress periodic vibrations. In [6], force sensors are integrated in the struts for decentralized force feedback while accelerometers fixed to the top platform are employed for centralized control.

Sensor fusion, the second approach (illustrated in Figure 1.1c), involves filtering signals from two sensors using complementary filters[1] that are subsequently summed to obtain an improved sensor signal. In [9], geophones (used at low frequency) are merged with force sensors (used at high frequency). It is demonstrated that combining both sensors using sensor fusion can improve performance compared to using the individual sensors independently. In [8], sensor fusion architecture is implemented with an accelerometer and a force sensor. This implementation is shown to simultaneously achieve high damping of structural modes (through the force sensors) while maintaining very low vibration transmissibility (through the accelerometers).

In [10], the performance of sensor fusion is compared with the more general case of "two-sensor control" (illustrated in Figure 1.1b). It is highlighted that "two-sensor control" provides greater control freedom, potentially enhancing performance. In [14], the use of force sensors and geophones is compared for vibration isolation purposes. Geophones are shown to provide better isolation performance than load cells but suffer from poor robustness. Conversely, the controller based on force sensors exhibited inferior performance (due to the presence of a pair of low frequency zeros), but demonstrated better robustness properties. A "two-sensor control" approach was proven to perform better than controllers based on individual sensors while maintaining better robustness. A Linear Quadratic Regulator (LQG) was employed to optimize the two-input/one-output controller.

Beyond these three main approaches, other control architectures have been proposed for different purposes. In [12], a first control loop utilizes force sensors and relative motion sensors to compensate for parasitic stiffness of the flexible joints. Subsequently, the system is decoupled in the modal space (facilitated by the removal of parasitic stiffness) and accelerometers are employed for vibration isolation.

The HAC-LAC architecture was previously investigated during the conceptual phase and successfully implemented to validate the NASS concept, demonstrating excellent performance. At the other end of the spectrum, the two-sensor approach yields greater control design freedom but introduces increased complexity in tuning, and thus was not pursued in this study. This work instead focuses on sensor fusion, which represents a promising middle ground between the proven HAC-LAC approach and the more complex two-sensor control strategy.

A review of sensor fusion is first presented (Section **??**), followed by an examination of the fundamental theoretical concepts (Section 1.2). In this section, both the robustness of the fusion and the noise characteristics of the resulting "super sensor" are derived and expressed as functions of the complementary filters' norms. A synthesis method for designing complementary filters that allow to shape their norms is proposed (Section 1.3). The investigation is then extended beyond the conventional two-sensor scenario, demonstrating how the proposed complementary filter synthesis can be generalized for applications requiring the fusion of three or more sensors (Section **??**).

[1] A set of two complementary filters are two transfer functions that sum to one.

## 1.1 Review of Sensor Fusion

Measuring a physical quantity using sensors is always subject to several limitations. First, the accuracy of the measurement is affected by various noise sources, such as electrical noise from the conditioning electronics. Second, the frequency range in which the measurement is relevant is bounded by the bandwidth of the sensor. One way to overcome these limitations is to combine several sensors using a technique called "sensor fusion" [18]. Fortunately, a wide variety of sensors exists, each with different characteristics. By carefully selecting the sensors to be fused, a "super sensor" is obtained that combines the benefits of the individual sensors.

In some applications, sensor fusion is employed to increase measurement bandwidth [19], [20], [21]. For instance, in [19], the bandwidth of a position sensor is extended by fusing it with an accelerometer that provides high-frequency motion information. In other applications, sensor fusion is utilized to obtain an estimate of the measured quantity with reduced noise [22], [23], [24], [25]. More recently, the fusion of sensors measuring different physical quantities has been proposed to enhance control properties [11], [26]. In [26], an inertial sensor used for active vibration isolation is fused with a sensor collocated with the actuator to improve the stability margins of the feedback controller.

On top of Stewart platforms, practical applications of sensor fusion are numerous. It is widely implemented for attitude estimation in autonomous vehicles such as unmanned aerial vehicles [27], [28], [29] and underwater vehicles [30], [31]. Sensor fusion offers significant benefits for high-performance positioning control as demonstrated in [11], [19], [20], [21]. It has also been identified as a key technology for improving the performance of active vibration isolation systems [8]. Emblematic examples include the isolation stages of gravitational wave detectors [26], [32] such as those employed at LIGO [22], [23] and Virgo [33].

Two principal methods are employed to perform sensor fusion: using complementary filters [34] or using Kalman filtering [35]. For sensor fusion applications, these methods share many relationships [25], [35], [36], [37]. However, Kalman filtering requires assumptions about the probabilistic characteristics of sensor noise [25], whereas complementary filters do not impose such requirements. Furthermore, complementary filters offer advantages over Kalman filtering for sensor fusion through their general applicability, low computational cost [36], and intuitive nature, as their effects can be readily interpreted in the frequency domain.

A set of filters is considered complementary if the sum of their transfer functions equals one at all frequencies. In early implementations of complementary filtering, analog circuits were used to physically realize the filters [34]. While analog complementary filters remain in use today [11], [38], digital implementation is now more common as it provides greater flexibility.

Various design methods have been developed to optimize complementary filters. The most straightforward approach utilizes analytical formulas. Depending on the application, these formulas may be of first order [11], [28], [39], second order [27], [29], [40], or higher orders [19], [20], [26], [40], [41].

Since the characteristics of the super sensor depend on the proper design of complementary filters [42], several optimization techniques have been developed. Some approaches focus on finding optimal parameters for analytical formulas [21], [29], [37], while others employ convex optimization tools [22], [23] such as linear matrix inequalities [30]. As demonstrated in [24], complementary filter design can be linked to the standard mixed-sensitivity control problem. Consequently, the powerful tools developed for classical control theory can be applied to complementary filter design. For example, in [29], the two gains of a Proportional Integral (PI) controller are optimized to minimize super sensor noise.

All these complementary filter design methods share the common objective of creating a super sensor

with desired characteristics, typically in terms of noise and dynamics. As reported in [20], [24], phase shifts and magnitude bumps in the super sensor dynamics may occur if complementary filters are poorly designed or if sensors are improperly calibrated. Therefore, the robustness of the fusion must be considered when designing complementary filters. Despite the numerous design methods proposed in the literature, a simple approach that specifies desired super sensor characteristics while ensuring good fusion robustness has been lacking.

Fortunately, both fusion robustness and super sensor characteristics can be linked to complementary filter magnitude [42]. Based on this relationship, the present work introduces an approach to designing complementary filters using $\mathcal{H}_\infty$ synthesis, which enables intuitive shaping of complementary filter magnitude in a straightforward manner.

## 1.2 Sensor Fusion and Complementary Filters Requirements

A general sensor fusion architecture using complementary filters is shown in Figure 1.2, where multiple sensors (in this case two) measure the same physical quantity $x$. The sensor output signals $\hat{x}_1$ and $\hat{x}_2$ represent estimates of $x$. These estimates are filtered by complementary filters and combined to form a new estimate $\hat{x}$.

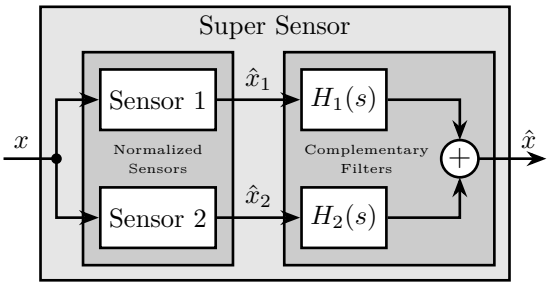


**Figure 1.2:** Schematic of a sensor fusion architecture using complementary filters.

The complementary property of filters $H_1(s)$ and $H_2(s)$ requires that the sum of their transfer functions equals one at all frequencies (1.1).

$$H_1(s) + H_2(s) = 1 \tag{1.1}$$

**Sensor Models and Sensor Normalization** To analyze sensor fusion architectures, appropriate sensor models are required. The model shown in Figure 1.3a consists of a linear time invariant (LTI) system $G_i(s)$ representing the sensor dynamics and an input $n_i$ representing sensor noise. The model input $x$ is the measured physical quantity, and its output $\tilde{x}_i$ is the "raw" output of the sensor.

Prior to filtering the sensor outputs $\tilde{x}_i$ with complementary filters, the sensors are typically normalized to simplify the fusion process. This normalization involves using an estimate $\hat{G}_i(s)$ of the sensor dynamics $G_i(s)$, and filtering the sensor output by the inverse of this estimate $\hat{G}_i^{-1}(s)$, as shown in Figure 1.3b. It is assumed that the sensor inverse $\hat{G}_i^{-1}(s)$ is proper and stable. This approach ensures that the units of the estimates $\hat{x}_i$ match the units of the physical quantity $x$. The sensor dynamics estimate $\hat{G}_i(s)$ may be a simple gain or a more complex transfer function.

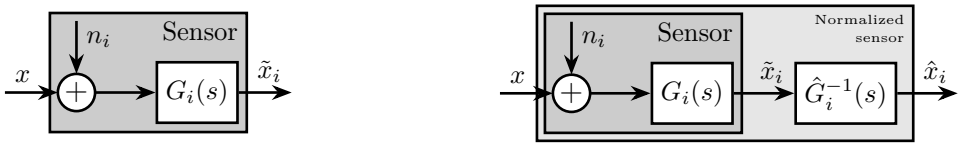


**(a)** Basic sensor model consisting of a noise input $n_i$ and a linear time invariant transfer function $G_i(s)$

**(b)** Normalized sensors using the inverse of an estimate $\hat{G}$

**Figure 1.3:** Sensor models with and without normalization.

Two normalized sensors are then combined to form a super sensor as shown in Figure 1.4. The two sensors measure the same physical quantity $x$ with dynamics $G_1(s)$ and $G_2(s)$, and with uncorrelated noises $n_1$ and $n_2$. The signals from both normalized sensors are fed into two complementary filters $H_1(s)$ and $H_2(s)$ and then combined to yield an estimate $\hat{x}$ of $x$. The super sensor output $\hat{x}$ is therefore described by (1.2).

$$\hat{x} = \Big(H_1(s)\hat{G}_1^{-1}(s)G_1(s) + H_2(s)\hat{G}_2^{-1}(s)G_2(s)\Big)x + H_1(s)\hat{G}_1^{-1}(s)G_1(s)n_1 + H_2(s)\hat{G}_2^{-1}(s)G_2(s)n_2 \quad (1.2)$$

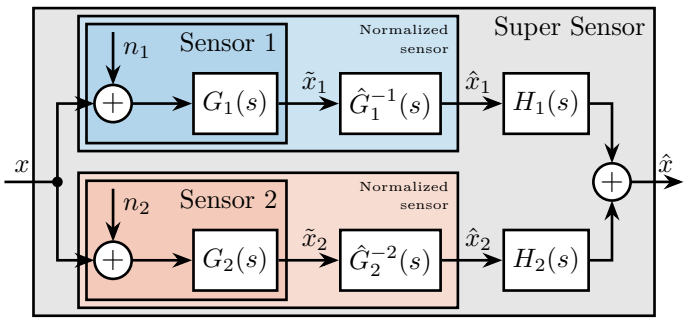


**Figure 1.4:** Sensor fusion architecture with two normalized sensors.

**Noise Sensor Filtering** First, consider the case where all sensors are perfectly normalized (1.3). The effects of imperfect normalization will be addressed subsequently.

$$\frac{\hat{x}_i}{x} = \hat{G}_i(s)G_i(s) = 1 \quad (1.3)$$

In that case, the super sensor output $\hat{x}$ equals $x$ plus the filtered noise from both sensors (1.4). From this equation, it is evident that the complementary filters $H_1(s)$ and $H_2(s)$ operate solely on the sensor noise. Thus, this sensor fusion architecture allows filtering of sensor noise without introducing distortion in the measured physical quantity. This fundamental property necessitates that the two filters must be complementary.

$$\hat{x} = x + H_1(s)n_1 + H_2(s)n_2 \quad (1.4)$$

The estimation error $\epsilon_x$, defined as the difference between the sensor output $\hat{x}$ and the measured quantity $x$, is computed for the super sensor (1.5).

$$\epsilon_x \triangleq \hat{x} - x = H_1(s)n_1 + H_2(s)n_2 \tag{1.5}$$

As shown in (1.6), the Power Spectral Density (PSD) of the estimation error $\Phi_{\epsilon_x}$ depends both on the norm of the two complementary filters and on the PSD of the noise sources $\Phi_{n_1}$ and $\Phi_{n_2}$.

$$\Phi_{\epsilon_x}(\omega) = |H_1(j\omega)|^2 \Phi_{n_1}(\omega) + |H_2(j\omega)|^2 \Phi_{n_2}(\omega) \tag{1.6}$$

If the two sensors have identical noise characteristics ($\Phi_{n_1}(\omega) = \Phi_{n_2}(\omega)$), simple averaging ($H_1(s) = H_2(s) = 0.5$) would minimize the super sensor noise. This represents the simplest form of sensor fusion using complementary filters.

However, sensors typically exhibit high noise levels in different frequency regions. In such cases, to reduce the noise of the super sensor, the norm $|H_1(j\omega)|$ should be minimized when $\Phi_{n_1}(\omega)$ exceeds $\Phi_{n_2}(\omega)$, and the norm $|H_2(j\omega)|$ should be minimized when $\Phi_{n_2}(\omega)$ exceeds $\Phi_{n_1}(\omega)$. Therefore, by appropriately shaping the norm of the complementary filters, the noise of the super sensor can be minimized.

**Sensor Fusion Robustness** In practical systems, sensor normalization is rarely perfect, and condition (1.3) is not fully satisfied.

To analyze such imperfections, a multiplicative input uncertainty is incorporated into the sensor dynamics (Figure 1.5a). The nominal model is the estimated model used for normalization $\hat{G}_i(s)$, $\Delta_i(s)$ is any stable transfer function satisfying $|\Delta_i(j\omega)| \leq 1$, $\forall\omega$, and $w_i(s)$ is a weighting transfer function representing the magnitude of uncertainty. The weight $w_i(s)$ is selected such that the actual sensor dynamics $G_i(j\omega)$ remains within the uncertain region represented by a circle in the complex plane, centered on 1 with a radius equal to $|w_i(j\omega)|$.

Since the nominal sensor dynamics is taken as the normalized filter, the normalized sensor model can be further simplified as shown in Figure 1.5b.

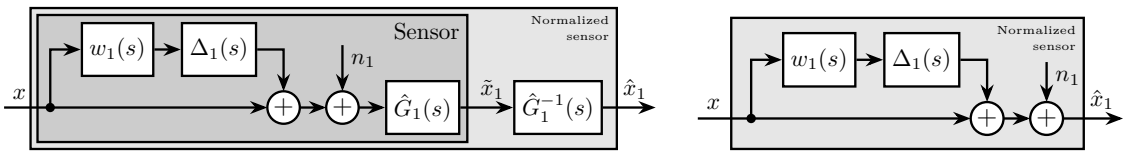


**(a)** Sensor with multiplicative input uncertainty **(b)** Simplified sensor model

**Figure 1.5:** Sensor models with dynamical uncertainty

The sensor fusion architecture incorporating sensor models with dynamical uncertainty is illustrated in Figure 1.6a. The super sensor dynamics (1.7) is no longer unity but depends on the sensor dynamical uncertainty weights $w_i(s)$ and the complementary filters $H_i(s)$. The dynamical uncertainty of the super sensor can be graphically represented in the complex plane by a circle centered on 1 with a radius equal to $|w_1(j\omega)H_1(j\omega)| + |w_2(j\omega)H_2(j\omega)|$ (Figure 1.6b).

The sensor fusion architecture with the sensor models including dynamical uncertainty is shown in Figure 1.6a. The super sensor dynamics (1.7) is no longer equal to 1 and now depends on the sensor dynamical uncertainty weights $w_i(s)$ as well as on the complementary filters $H_i(s)$. The dynamical

uncertainty of the super sensor can be graphically represented in the complex plane by a circle centered on 1 with a radius equal to $|w_1(j\omega)H_1(j\omega)| + |w_2(j\omega)H_2(j\omega)|$ (Figure 1.6b).

$$\frac{\hat{x}}{x} = 1 + w_1(s)H_1(s)\Delta_1(s) + w_2(s)H_2(s)\Delta_2(s) \tag{1.7}$$

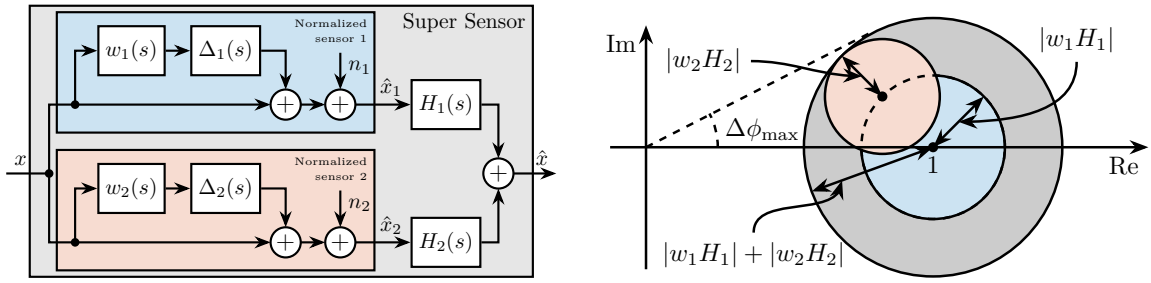


**(a)** Sensor Fusion Architecture

**(b)** Uncertainty regions

**Figure 1.6:** Sensor fusion architecture with sensor dynamics uncertainty (a). Uncertainty region (b) of the super sensor dynamics in the complex plane (grey circle). The contribution of both sensors 1 and 2 to the total uncertainty are represented respectively by a blue circle and a red circle. The frequency dependency $\omega$ is here omitted.

The super sensor dynamical uncertainty, and consequently the robustness of the fusion, clearly depends on the complementary filters' norm. As it is generally desired to limit the dynamical uncertainty of the super sensor, the norm of the complementary filter $|H_i(j\omega)|$ should be made small when $|w_i(j\omega)|$ is large, i.e., at frequencies where the sensor dynamics is uncertain.

## 1.3 Complementary Filters Shaping

As demonstrated in Section 1.2, both the noise characteristics and robustness of the super sensor are functions of the complementary filters' norm. Consequently, a synthesis method that enables precise shaping of complementary filter norms would provide significant practical benefits. In this section, such a synthesis approach is developed by formulating the design objective as a standard $\mathcal{H}_\infty$ optimization problem. The proper design of weighting functions, which are used to specify the desired complementary filter shapes during synthesis, is discussed in detail. Finally, the efficacy of the proposed synthesis method is validated through a simple example.

**Synthesis Objective** The primary objective is to shape the norms of two filters $H_1(s)$ and $H_2(s)$ while ensuring they maintain their complementary property as defined in (1.1). This is equivalent to finding proper and stable transfer functions $H_1(s)$ and $H_2(s)$ that satisfy conditions (1.9a), (1.9b), and (1.9c). The functions $W_1(s)$ and $W_2(s)$ represent weighting transfer functions that are carefully selected to specify the maximum desired norm of the complementary filters during synthesis.

$$H_1(s) + H_2(s) = 1 \tag{1.8a}$$

$$|H_1(j\omega)| \leq \frac{1}{|W_1(j\omega)|} \quad \forall\omega \tag{1.8b}$$

$$|H_2(j\omega)| \leq \frac{1}{|W_2(j\omega)|} \quad \forall\omega \tag{1.8c}$$

**Shaping of Complementary Filters using $\mathcal{H}_\infty$ synthesis** The synthesis objective can be readily expressed as a standard $\mathcal{H}_\infty$ optimization problem and solved using widely available computational tools. Consider the generalized plant $P(s)$ illustrated in Figure 1.7a and mathematically described by (1.10).

$$\begin{bmatrix} z_1 \\ z_2 \\ v \end{bmatrix} = P(s) \begin{bmatrix} w \\ u \end{bmatrix}; \quad P(s) = \begin{bmatrix} W_1(s) & -W_1(s) \\ 0 & W_2(s) \\ 1 & 0 \end{bmatrix} \tag{1.9}$$

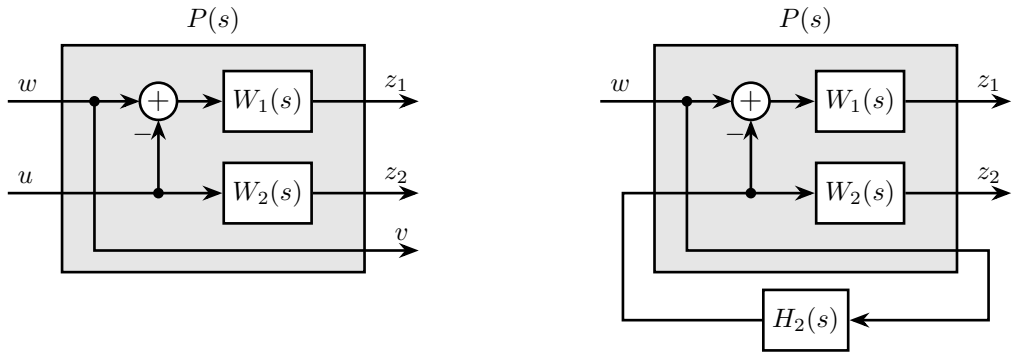


**(a)** Generalized plant

**(b)** Generalized plant with the synthesized filter

**Figure 1.7:** Architecture for the $\mathcal{H}_\infty$ synthesis of complementary filters

Applying standard $\mathcal{H}_\infty$ synthesis to the generalized plant $P(s)$ is equivalent to finding a stable filter $H_2(s)$ that, based on input $v$, generates an output signal $u$ such that the $\mathcal{H}_\infty$ norm of the system shown in Figure 1.7b from $w$ to $[z_1,\ z_2]$ does not exceed unity, as expressed in (1.11).

$$\left\| \begin{matrix} (1 - H_2(s))\, W_1(s) \\ H_2(s) W_2(s) \end{matrix} \right\|_\infty \leq 1 \tag{1.10}$$

By defining $H_1(s)$ as the complement of $H_2(s)$ ((1.12)), the $\mathcal{H}_\infty$ synthesis objective becomes equivalent to (1.13), ensuring that conditions (1.9b) and (1.9c) are satisfied.

$$H_1(s) \triangleq 1 - H_2(s) \tag{1.11}$$

$$\left\| \begin{matrix} H_1(s) W_1(s) \\ H_2(s) W_2(s) \end{matrix} \right\|_\infty \leq 1 \tag{1.12}$$

Therefore, applying $\mathcal{H}_\infty$ synthesis to the standard plant $P(s)$ ((1.10)) generates two filters, $H_2(s)$ and $H_1(s) \triangleq 1 - H_2(s)$, that are complementary as required by (1.9), with norms bounded by the specified constraints in (1.9b) and (1.9c).

It should be noted that there exists only an implication (not an equivalence) between the $\mathcal{H}_\infty$ norm condition in (1.13) and the initial synthesis objectives in (1.9b) and (1.9c). Consequently, the optimization may be somewhat conservative with respect to the set of filters on which it operates (see [43, Chap. 2.8.3]).

**Weighting Functions Design** Weighting functions play a crucial role during synthesis by specifying the maximum allowable norms for the complementary filters. The proper design of these weighting functions is essential for the successful implementation of the proposed $\mathcal{H}_\infty$ synthesis approach.

Three key considerations should guide the design of weighting functions. First, only proper and stable transfer functions should be employed. Second, the order of the weighting functions should remain reasonably small to minimize computational costs associated with solving the optimization problem and to facilitate practical implementation of the filters (as the order of the synthesized filters equals the sum of the weighting functions' orders). Third, the fundamental limitations imposed by the complementary property ((1.1)) must be respected, which implies that $|H_1(j\omega)|$ and $|H_2(j\omega)|$ cannot both be made small at the same frequency.

When designing complementary filters, it is typically desirable to specify their slopes, "blending" frequency, and maximum gains at low and high frequencies. To facilitate the expression of these specifications, formula (1.14) is proposed for the design of weighting functions. The parameters in this formula are $G_0 = \lim_{\omega\to 0} |W(j\omega)|$ (the low-frequency gain), $G_\infty = \lim_{\omega\to\infty} |W(j\omega)|$ (the high-frequency gain), $G_c = |W(j\omega_c)|$ (the gain at a specific frequency $\omega_c$ in rad/s), and $n$ (the slope between high and low frequency, which also corresponds to the order of the weighting function). The typical magnitude response of a weighting function generated using (1.14) is illustrated in Figure 1.8.

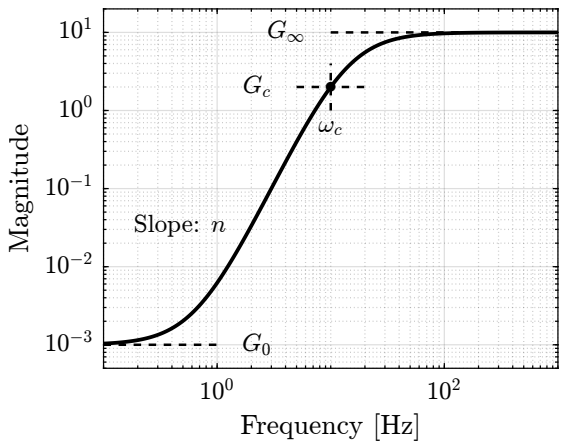


**Figure 1.8:** Magnitude of a weighting function generated using (1.14), $G_0 = 10^{-3}$, $G_\infty = 10$, $\omega_c = 10\,\text{Hz}$, $G_c = 2$, $n = 3$.

$$W(s) = \left( \frac{\frac{1}{\omega_c}\sqrt{\frac{1-\left(\frac{G_0}{G_c}\right)^{\frac{2}{n}}}{1-\left(\frac{G_c}{G_\infty}\right)^{\frac{2}{n}}}}\, s + \left(\frac{G_0}{G_c}\right)^{\frac{1}{n}}}{\left(\frac{1}{G_\infty}\right)^{\frac{1}{n}} \frac{1}{\omega_c}\sqrt{\frac{1-\left(\frac{G_0}{G_c}\right)^{\frac{2}{n}}}{1-\left(\frac{G_c}{G_\infty}\right)^{\frac{2}{n}}}}\, s + \left(\frac{1}{G_c}\right)^{\frac{1}{n}}} \right)^n \tag{1.13}$$

**Validation of the proposed synthesis method** The proposed methodology for designing complementary filters is now applied to a simple example. Consider the design of two complementary filters $H_1(s)$ and $H_2(s)$ with the following requirements:

- The blending frequency should be approximately 10 Hz
- The slope of $|H_1(j\omega)|$ should be $+2$ below 10 Hz, with a low-frequency gain of $10^{-3}$
- The slope of $|H_2(j\omega)|$ should be $-3$ above 10 Hz, with a high-frequency gain of $10^{-3}$

The first step involves translating these requirements by appropriately designing the weighting functions. The formula proposed in (1.14) is employed for this purpose. The parameters used are summarized in Table 1.2. The inverse magnitudes of the designed weighting functions, which represent the maximum allowable norms of the complementary filters, are depicted by the dashed lines in Figure 1.9.

| Parameter | $W_1(s)$ | $W_2(s)$ |
|---|---|---|
| $G_0$ | 0.1 | 1000 |
| $G_\infty$ | 1000 | 0.1 |
| $\omega_c$ | $2\pi \cdot 10$ | $2\pi \cdot 10$ |
| $G_c$ | 0.45 | 0.45 |
| $n$ | 2 | 3 |

**Table 1.1:** Parameters for $W_1(s)$ and $W_2(s)$

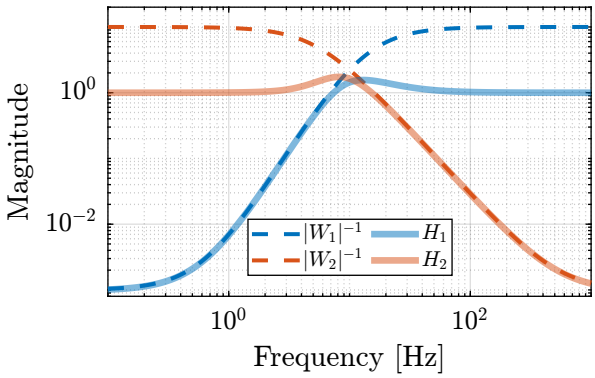


**Figure 1.9:** Weights and obtained filters

Standard $\mathcal{H}_\infty$ synthesis is then applied to the generalized plant shown in Figure 1.7a. This yields the filter $H_2(s)$ that minimizes the $\mathcal{H}_\infty$ norm from input $w$ to outputs $[z_1,\ z_2]^\intercal$. The resulting $\mathcal{H}_\infty$ norm is found to be close to unity, indicating successful synthesis: the norms of the complementary filters remain below the specified upper bounds. This is confirmed by the Bode plots of the obtained complementary filters in Figure 1.9. This straightforward example demonstrates that the proposed methodology for shaping complementary filters is both simple and effective.

## 1.4 Synthesis of a set of three complementary filters

Some applications require merging more than two sensors [37], [40]. For instance, at LIGO, three sensors (an LVDT, a seismometer, and a geophone) are merged to form a super sensor [41].

When merging $n > 2$ sensors using complementary filters, two architectures can be employed as shown in Figure 1.10. The fusion can be performed either in a "sequential" manner where $n-1$ sets of two complementary filters are used (Figure 1.10a), or in a "parallel" manner where one set of $n$ complementary filters is used (Figure 1.10b).

In the sequential approach, typical sensor fusion synthesis techniques can be applied. However, when a parallel architecture is implemented, a new synthesis method for a set of more than two complementary filters is required, as only simple analytical formulas have been proposed in the literature [37], [40]. A generalization of the proposed complementary filter synthesis method is presented in this section.

The synthesis objective is to compute a set of $n$ stable transfer functions $[H_1(s),\ H_2(s),\ \ldots,\ H_n(s)]$ that satisfy conditions (1.15a) and (1.15b).

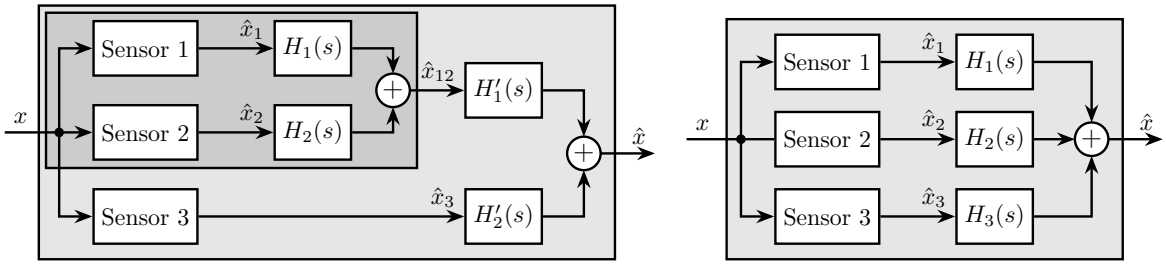


**(a)** Sequential fusion

**(b)** Parallel fusion

**Figure 1.10:** Possible sensor fusion architecture when more than two sensors are to be merged

$$\sum_{i=1}^{n} H_i(s) = 1 \tag{1.14a}$$

$$|H_i(j\omega)| < \frac{1}{|W_i(j\omega)|}, \quad \forall\omega,\ i = 1 \dots n \tag{1.14b}$$

The transfer functions $[W_1(s),\ W_2(s),\ \dots,\ W_n(s)]$ are weights selected to specify the maximum complementary filters' norm during synthesis.

This synthesis objective is closely related to the one described in Section 1.3, and the proposed synthesis method represents a generalization of the approach previously presented. A set of $n$ complementary filters can be shaped by applying standard $\mathcal{H}_\infty$ synthesis to the generalized plant $P_n(s)$ described by (1.16).

$$\begin{bmatrix} z_1 \\ \vdots \\ z_n \\ v \end{bmatrix} = P_n(s) \begin{bmatrix} w \\ u_1 \\ \vdots \\ u_{n-1} \end{bmatrix}; \quad P_n(s) = \begin{bmatrix} W_1 & -W_1 & \dots & \dots & -W_1 \\ 0 & W_2 & 0 & \dots & 0 \\ \vdots & \ddots & \ddots & \ddots & \vdots \\ \vdots & & \ddots & \ddots & 0 \\ 0 & \dots & \dots & 0 & W_n \\ 1 & 0 & \dots & \dots & 0 \end{bmatrix} \tag{1.15}$$

If the synthesis is successful, a set of $n-1$ filters $[H_2(s),\ H_3(s),\ \dots,\ H_n(s)]$ is obtained such that (1.17) is satisfied.

$$\left\| \begin{matrix} (1 - [H_2(s) + H_3(s) + \dots + H_n(s)])\, W_1(s) \\ H_2(s)W_2(s) \\ \vdots \\ H_n(s)W_n(s) \end{matrix} \right\|_\infty \leq 1 \tag{1.16}$$

$H_1(s)$ is then defined using (1.18), which ensures the complementary property for the set of $n$ filters (1.15a). Condition (1.15b) is satisfied through (1.17).

$$H_1(s) \triangleq 1 - \left[H_2(s) + H_3(s) + \cdots + H_n(s)\right] \tag{1.17}$$

To validate the proposed method for synthesizing a set of three complementary filters, an example is provided. The sensors to be merged are a displacement sensor (effective from DC up to 1 Hz), a geophone (effective from 1 to 10 Hz), and an accelerometer (effective above 10 Hz). Three weighting functions are designed using formula (1.14), and their inverse magnitudes are shown in Figure 1.11b (dashed curves).

Consider the generalized plant $P_3(s)$ shown in Figure 1.11a, which is also described by (1.19).

$$\begin{bmatrix} z_1 \\ z_2 \\ z_3 \\ v \end{bmatrix} = P_3(s) \begin{bmatrix} w \\ u_1 \\ u_2 \end{bmatrix}; \quad P_3(s) = \begin{bmatrix} W_1(s) & -W_1(s) & -W_1(s) \\ 0 & W_2(s) & 0 \\ 0 & 0 & W_3(s) \\ 1 & 0 & 0 \end{bmatrix} \tag{1.18}$$

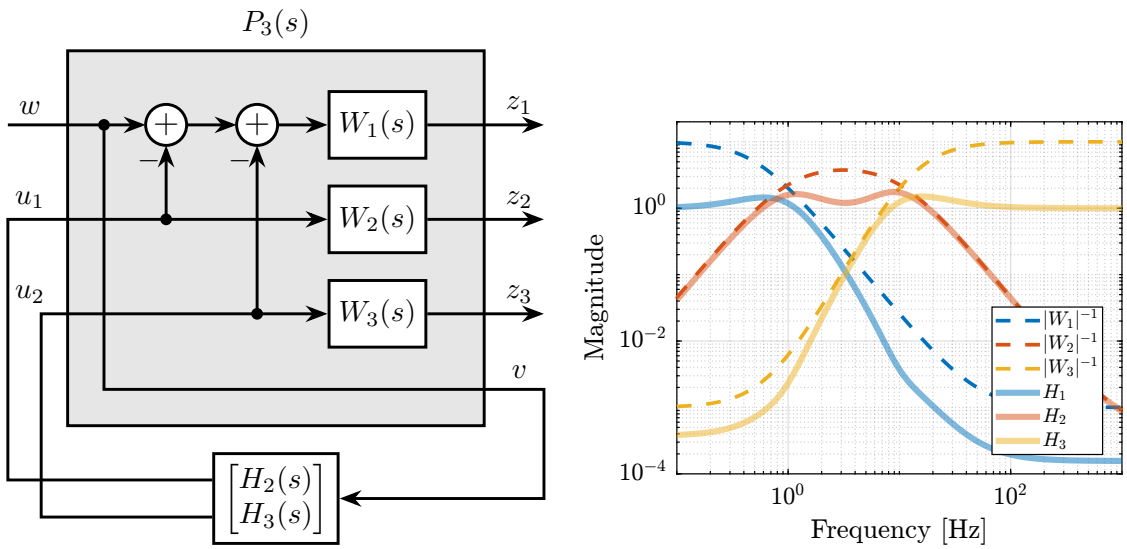


**(a)** Generalized plant with the synthesized filter

**(b)** Weights and obtained filters

**Figure 1.11:** Architecture for the $\mathcal{H}_\infty$ synthesis of three complementary filters (a). Bode plot of the inverse weighting functions and of the three obtained complementary filters (b)

Standard $\mathcal{H}_\infty$ synthesis is performed on the generalized plant $P_3(s)$. Two filters, $H_2(s)$ and $H_3(s)$, are obtained such that the $\mathcal{H}_\infty$ norm of the closed-loop transfer from $w$ to $[z_1,\ z_2,\ z_3]$ of the system in Figure 1.11a is less than one. Filter $H_1(s)$ is defined using (1.20), thus ensuring the complementary property of the obtained set of filters.

$$H_1(s) \triangleq 1 - \left[H_2(s) + H_3(s)\right] \tag{1.19}$$

Figure 1.11b displays the three synthesized complementary filters (solid lines), confirming the successful synthesis.

# Conclusion

A new method for designing complementary filters using the $\mathcal{H}_\infty$ synthesis has been proposed. This approach allows shaping of the filter magnitudes through the use of weighting functions during synthesis. This capability is particularly valuable in practice since the characteristics of the super sensor are directly linked to the complementary filters' magnitude. Consequently, typical sensor fusion objectives can be effectively translated into requirements on the magnitudes of the filters.

For the Nano Active Stabilization System (NASS), the High Authority Control-Integral Force Feedback (HAC-IFF) strategy was found to perform well and to offer the advantages of being both intuitive to understand and straightforward to tune. Looking forward, it would be interesting to investigate how sensor fusion (particularly between the force sensor and external metrology) compares to the HAC-IFF approach in terms of performance and robustness.

# 2 Decoupling

When dealing with MIMO systems, a typical strategy is to:

- First decouple the plant dynamics (discussed in this section)
- Apply SISO control for the decoupled plant (discussed in section 3)

Another strategy would be to apply a multivariable control synthesis to the coupled system. Strangely, while H-infinity synthesis is a mature technology, it use for the control of Stewart platform is not yet demonstrated. From [14]:

> xperimental closed-loop control results using the hexapod have shown that controllers designed using a decentralized single-strut design work well when compared to full multivariable methodologies.

☒ Review of Decoupling Strategies for stewart platforms

☐ Add some citations about different methods

☐ Maybe transform table into text

**Table 2.1:** Litterature review about decoupling strategy for Stewart platform control

| Actuators | Sensors | Control |
|---|---|---|
| APA | Eddy current displacement | **Decentralized** (struts) PI + LPF control |
| PZT | Strain Gauge | Decentralized position feedback |
| Piezo | | |
| Voice Coil | Force | **Cartesian frame** decoupling |
| Voice Coil | Force | Cartesian Frame, Jacobians, IFF |
| Hydraulic | LVDT | Decentralized (strut) vs Centralized (cartesian) |
| Voice Coil | Accelerometer (collocated), ext. Rx/Ry sensors | Cartesian acceleration feedback (isolation) + 2DoF pointing control (external sens |
| Voice Coil | Accelerometer in each leg | Centralized Vibration Control, PI, Skyhook |
| Voice Coil | Geophone + Eddy Current (Struts, collocated) | Decentralized (Sky Hook) + Centralized (**modal**) Control |
| Piezoelectric | Force, Position | Vibration isolation, Model-Based, **Modal control**: 6x PI controllers |
| PZT | Geophone (struts) | **H-Infinity** and mu-synthesis |
| Voice Coil | Force sensors (struts) + accelerometer (cartesian) | Decentralized Force Feedback + Centralized H2 control based on accelerometers |
| Voice Coil | Accelerometers | MIMO H-Infinity, active damping |

The goal of this section is to compare the use of several methods for the decoupling of parallel manipulators.

It is structured as follow:

- Section 2.1: the model used to compare/test decoupling strategies is presented
- Section 2.3: decoupling using Jacobian matrices is presented
- Section 2.4: modal decoupling is presented
- Section 2.5: SVD decoupling is presented
- Section 2.6: the three decoupling methods are applied on the test model and compared
- Conclusions are drawn on the three decoupling methods

## 2.1 Test Model

- Instead of comparing the decoupling strategies using the Stewart platform, a similar yet much simpler parallel manipulator is used instead
- to render the analysis simpler, the system of Figure 2.1 is used
- Fully parallel manipulator: it has 3DoF, and has 3 parallels struts whose model is shown in Figure 2.1b As many DoF as actuators and sensors
- It is quite similar to the Stewart platform (parallel architecture, as many struts as DoF)

Two frames are defined:

- $\{M\}$ with origin $O_M$ at the Center of mass of the solid body
- $\{K\}$ with origin $O_K$ at the Center of mass of the parallel manipulator

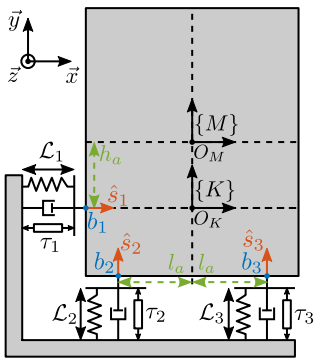


**(a)** Geometrical parameters

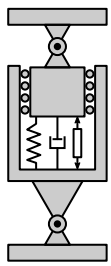

**(b)** Strut model

**Figure 2.1:** 3DoF model used to study decoupling strategies

First, the equation of motion are derived. Expressing the second law of Newton on the suspended mass, expressed at its center of mass gives

$$\boldsymbol{M}_{\{M\}}\ddot{\boldsymbol{\mathcal{X}}}_{\{M\}}(t) = \sum \boldsymbol{\mathcal{F}}_{\{M\}}(t) \tag{2.1}$$

with $\boldsymbol{\mathcal{X}}_{\{M\}}$ the two translation and one rotation expressed with respect to the center of mass and $\boldsymbol{\mathcal{F}}_{\{M\}}$ forces and torque applied at the center of mass.

$$\boldsymbol{\mathcal{X}}_{\{M\}} = \begin{bmatrix} x \\ y \\ R_z \end{bmatrix}, \quad \boldsymbol{\mathcal{F}}_{\{M\}} = \begin{bmatrix} F_x \\ F_y \\ M_z \end{bmatrix} \tag{2.2}$$

In order to map the spring, damping and actuator forces to XY forces and Z torque expressed at the center of mass, the Jacobian matrix $\boldsymbol{J}_{\{M\}}$ is used.

$$\boldsymbol{J}_{\{M\}} = \begin{bmatrix} 1 & 0 & h_a \\ 0 & 1 & -l_a \\ 0 & 1 & l_a \end{bmatrix} \tag{2.3}$$

Then, the equation of motion linking the actuator forces $\tau$ to the motion of the mass $\boldsymbol{\mathcal{X}}_{\{M\}}$ is obtained.

$$\boldsymbol{M}_{\{M\}}\ddot{\boldsymbol{\mathcal{X}}}_{\{M\}}(t) + \boldsymbol{J}_{\{M\}}^{\intercal}\boldsymbol{\mathcal{C}}\boldsymbol{J}_{\{M\}}\dot{\boldsymbol{\mathcal{X}}}_{\{M\}}(t) + \boldsymbol{J}_{\{M\}}^{\intercal}\boldsymbol{\mathcal{K}}\boldsymbol{J}_{\{M\}}\boldsymbol{\mathcal{X}}_{\{M\}}(t) = \boldsymbol{J}_{\{M\}}^{\intercal}\boldsymbol{\tau}(t) \tag{2.4}$$

Matrices representing the payload inertia as well as the actuator stiffness and damping are shown in

$$\boldsymbol{M}_{\{M\}} = \begin{bmatrix} m & 0 & 0 \\ 0 & m & 0 \\ 0 & 0 & I \end{bmatrix}, \quad \boldsymbol{\mathcal{K}} = \begin{bmatrix} k & 0 & 0 \\ 0 & k & 0 \\ 0 & 0 & k \end{bmatrix}, \quad \boldsymbol{\mathcal{C}} = \begin{bmatrix} c & 0 & 0 \\ 0 & c & 0 \\ 0 & 0 & c \end{bmatrix} \tag{2.5}$$

Parameters used for the following analysis are summarized in table 2.2.

**Table 2.2:** Model parameters

| Parameter | Description | Value |
|---|---|---|
| $l_a$ | | $0.5\,m$ |
| $h_a$ | | $0.2\,m$ |
| $k$ | Actuator stiffness | $10\,N/\mu m$ |
| $c$ | Actuator damping | $200\,Ns/m$ |
| $m$ | Payload mass | $40\,\mathrm{kg}$ |
| $I$ | Payload rotational inertia | $5\,\mathrm{kg}m^2$ |

## 2.2 Control in the frame of the struts

Let's first study the obtained dynamics in the frame of the struts. The equation of motion linking actuator forces $\boldsymbol{\tau}$ to strut relative motion $\boldsymbol{\mathcal{L}}$ is obtained from (2.4) by mapping the cartesian motion of the mass to the relative motion of the struts using the Jacobian matrix $\boldsymbol{J}_{\{M\}}$ (2.3) .

The transfer function from $\boldsymbol{\tau}$ to $\boldsymbol{\mathcal{L}}$ is shown in equation (2.6).

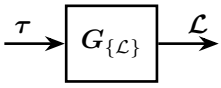


$$\frac{\boldsymbol{\mathcal{L}}}{\boldsymbol{\tau}}(s) = \boldsymbol{G}_{\mathcal{L}}(s) = \left(\boldsymbol{J}_{\{M\}}^{-\intercal}\boldsymbol{M}_{\{M\}}\boldsymbol{J}_{\{M\}}^{-1}s^2 + \boldsymbol{\mathcal{C}}s + \boldsymbol{\mathcal{K}}\right)^{-1} \tag{2.6}$$

At low frequency the plant converges to a diagonal constant matrix whose diagonal elements are linked to the actuator stiffnesses (2.7).

$$\boldsymbol{G}_{\mathcal{L}}(j\omega) \xrightarrow[\omega \to 0]{} \boldsymbol{\mathcal{K}}^{-1} \tag{2.7}$$

At high frequency, the plant converges to the mass matrix mapped in the frame of the struts, which is in general highly non-diagonal.

The magnitude of the coupled plant $\boldsymbol{G}_{\mathcal{L}}$ is shown in Figure 2.2. This confirms that at low frequency (below the first suspension mode), the plant is well decoupled. Depending on the symmetry in the system, some diagonal elements may be equal (such as for struts 2 and 3 in this example).

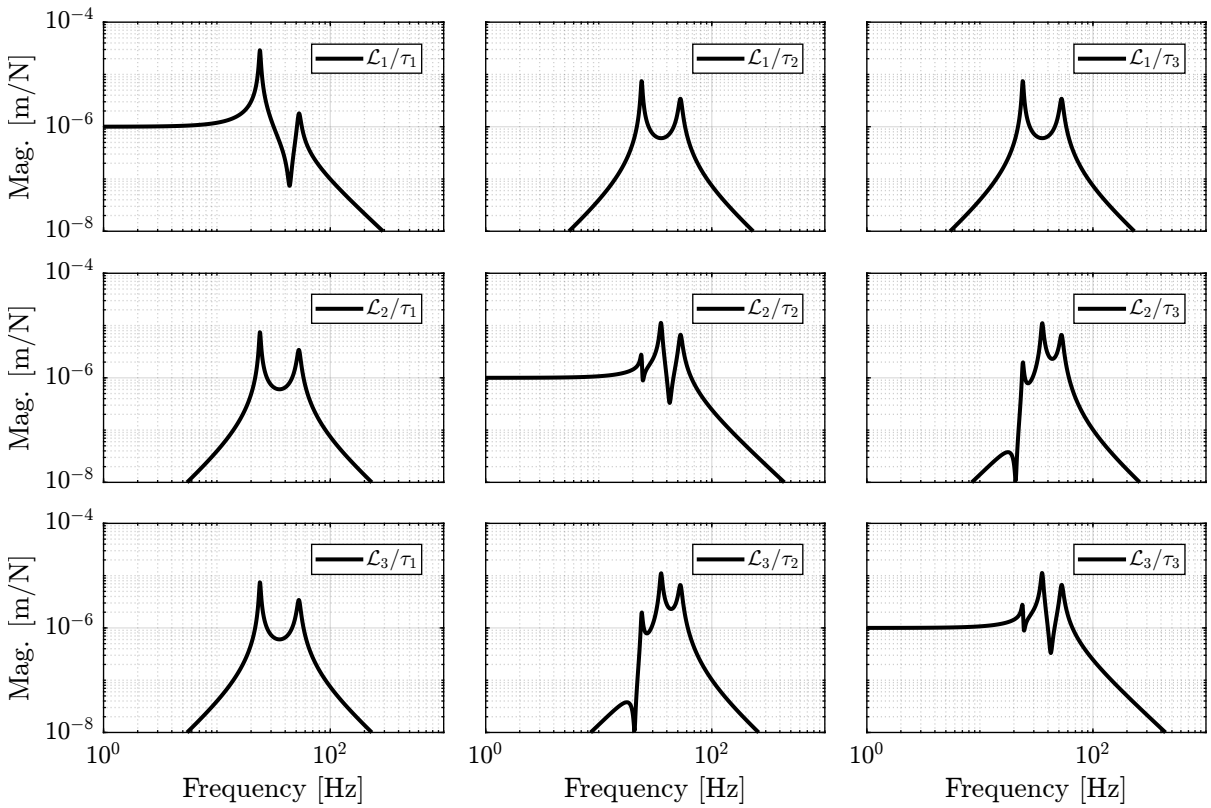


**Figure 2.2:** Magnitude of the coupled plant.

## 2.3 Jacobian Decoupling

**Jacobian Matrix** As already explained, the Jacobian matrix can be used to both convert strut velocity $\dot{\mathcal{L}}$ to payload velocity and angular velocity $\dot{\mathcal{X}}_{\{O\}}$ and Convert actuators forces $\boldsymbol{\tau}$ to forces/torque applied on the payload $\boldsymbol{\mathcal{F}}_{\{O\}}$ (2.8).

$$\dot{\boldsymbol{\mathcal{X}}}_{\{O\}} = \boldsymbol{J}_{\{O\}}\dot{\boldsymbol{\mathcal{L}}}, \quad \dot{\boldsymbol{\mathcal{L}}} = \boldsymbol{J}_{\{O\}}^{-1}\dot{\boldsymbol{\mathcal{X}}}_{\{O\}} \tag{2.8a}$$

$$\boldsymbol{\mathcal{F}}_{\{O\}} = \boldsymbol{J}_{\{O\}}^{\intercal}\boldsymbol{\tau}, \quad \boldsymbol{\tau} = \boldsymbol{J}_{\{O\}}^{-\intercal}\boldsymbol{\mathcal{F}}_{\{O\}} \tag{2.8b}$$

The obtained plan (Figure 2.3) has inputs and outputs that have physical meaning:

- $\boldsymbol{\mathcal{F}}_{\{O\}}$ are forces/torques applied on the payload at the origin of frame $\{O\}$
- $\boldsymbol{\mathcal{X}}_{\{O\}}$ are translations/rotation of the payload expressed in frame $\{O\}$

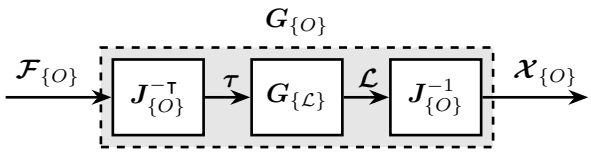


**Figure 2.3:** Block diagram of the transfer function from $\boldsymbol{\mathcal{F}}_{\{O\}}$ to $\boldsymbol{\mathcal{X}}_{\{O\}}$

$$\frac{\boldsymbol{\mathcal{X}}_{\{O\}}}{\boldsymbol{\mathcal{F}}_{\{O\}}}(s) = \boldsymbol{G}_{\{O\}}(s) = \left(\boldsymbol{J}_{\{O\}}^{\intercal}\boldsymbol{J}_{\{M\}}^{-\intercal}\boldsymbol{M}_{\{M\}}\boldsymbol{J}_{\{M\}}^{-1}\boldsymbol{J}_{\{O\}}s^2 + \boldsymbol{J}_{\{O\}}^{\intercal}\boldsymbol{\mathcal{C}}\boldsymbol{J}_{\{O\}}s + \boldsymbol{J}_{\{O\}}^{\intercal}\boldsymbol{\mathcal{K}}\boldsymbol{J}_{\{O\}}\right)^{-1} \tag{2.9}$$

The frame $\{O\}$ can be any chosen frame, but the decoupling properties depends on the chosen frame $\{O\}$. There are two natural choices: the center of mass $\{M\}$ and the center of stiffness $\{K\}$. Note that the Jacobian matrix is only based on the geometry of the system and does not depend on the physical properties such as mass and stiffness.

**Center Of Mass** If the center of mass is chosen as the decoupling frame. The Jacobian matrix and its inverse are expressed in (2.10).

$$\boldsymbol{J}_{\{M\}} = \begin{bmatrix} 1 & 0 & h_a \\ 0 & 1 & -l_a \\ 0 & 1 & l_a \end{bmatrix}, \quad \boldsymbol{J}_{\{M\}}^{-1} = \begin{bmatrix} 1 & \frac{h_a}{2l_a} & \frac{-h_a}{2l_a} \\ 0 & \frac{1}{2} & \frac{1}{2} \\ 0 & \frac{-1}{2l_a} & \frac{1}{2l_a} \end{bmatrix} \tag{2.10}$$

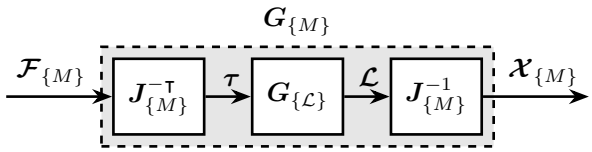

Analytical formula of the plant is (2.11).

$$\frac{\boldsymbol{\mathcal{X}}_{\{M\}}}{\boldsymbol{\mathcal{F}}_{\{M\}}}(s) = \boldsymbol{G}_{\{M\}}(s) = \left(\boldsymbol{M}_{\{M\}}s^2 + \boldsymbol{J}_{\{M\}}^{\intercal}\boldsymbol{\mathcal{C}}\boldsymbol{J}_{\{M\}}s + \boldsymbol{J}_{\{M\}}^{\intercal}\boldsymbol{\mathcal{K}}\boldsymbol{J}_{\{M\}}\right)^{-1} \tag{2.11}$$

At high frequency, converges towards the inverse of the mass matrix, which is a diagonal matrix (2.12).

$$\boldsymbol{G}_{\{M\}}(j\omega) \xrightarrow[\omega\to\infty]{} -\omega^2\boldsymbol{M}_{\{M\}}^{-1} = -\omega^2\begin{bmatrix} 1/m & 0 & 0 \\ 0 & 1/m & 0 \\ 0 & 0 & 1/I \end{bmatrix} \tag{2.12}$$

Plant is therefore well decoupled above the suspension mode with the highest frequency. Such strategy is usually applied on systems with low frequency suspension modes, such that the plant corresponds to decoupled mass lines.

☐ Reference to some papers about vibration isolation or ASML?

The coupling at low frequency can easily be understood physically. When a static (or with frequency lower than the suspension modes) force is applied at the center of mass, rotation is induced by the stiffness of the first actuator, not in line with the force application point. this is illustrated in Figure 2.4b.

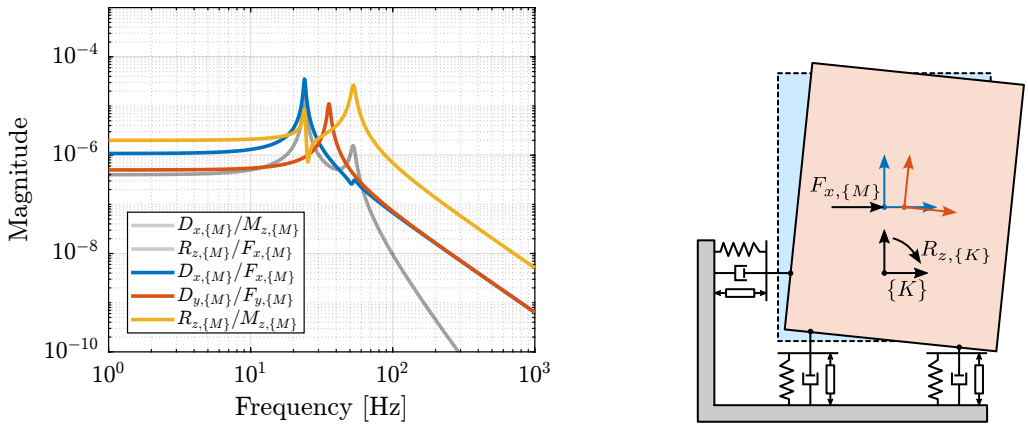


**(a)** Dynamics at the CoM

**(b)** Static force applied at the CoM

**Figure 2.4:** Plant decoupled using the Jacobian matrix expresssed at the center of mass (a). The physical reason for low frequency coupling is illustrated in (b).

### Center Of Stiffness

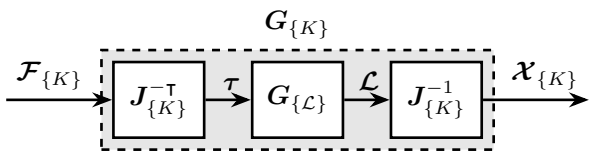

$$\boldsymbol{J}_{\{K\}} = \begin{bmatrix} 1 & 0 & 0 \\ 0 & 1 & -l_a \\ 0 & 1 & l_a \end{bmatrix}, \quad \boldsymbol{J}_{\{K\}}^{-1} = \begin{bmatrix} 1 & 0 & 0 \\ 0 & \frac{1}{2} & \frac{1}{2} \\ 0 & \frac{-1}{2l_a} & \frac{1}{2l_a} \end{bmatrix} \tag{2.13}$$

Frame $\{K\}$ is chosen such that $\boldsymbol{J}_{\{K\}}^{\intercal}\boldsymbol{\mathcal{K}}\boldsymbol{J}_{\{K\}}$ is diagonal. Typically, it can me made based on physical reasoning as is the case here.

$$\frac{\boldsymbol{\mathcal{X}}_{\{K\}}}{\boldsymbol{\mathcal{F}}_{\{K\}}}(s) = \boldsymbol{G}_{\{K\}}(s) = \left(\boldsymbol{J}_{\{K\}}^{\intercal}\boldsymbol{J}_{\{M\}}^{-\intercal}\boldsymbol{M}_{\{M\}}\boldsymbol{J}_{\{M\}}^{-1}\boldsymbol{J}_{\{K\}}s^2 + \boldsymbol{J}_{\{K\}}^{\intercal}\boldsymbol{\mathcal{C}}\boldsymbol{J}_{\{K\}}s + \boldsymbol{J}_{\{K\}}^{\intercal}\boldsymbol{\mathcal{K}}\boldsymbol{J}_{\{K\}}\right)^{-1} \tag{2.14}$$

Plant is well decoupled below the suspension mode with the lowest frequency. This is usually suited for systems which high stiffness.

$$\boldsymbol{G}_{\{K\}}(j\omega) \xrightarrow[\omega \to 0]{} \boldsymbol{J}_{\{K\}}^{-1}\boldsymbol{\mathcal{K}}^{-1}\boldsymbol{J}_{\{K\}}^{-\intercal} \tag{2.15}$$

The physical reason for high frequency coupling is schematically shown in Figure 2.5b. At high frequency, a force applied on a point which is not aligned with the center of mass. Therefore, it will induce some rotation around the center of mass.

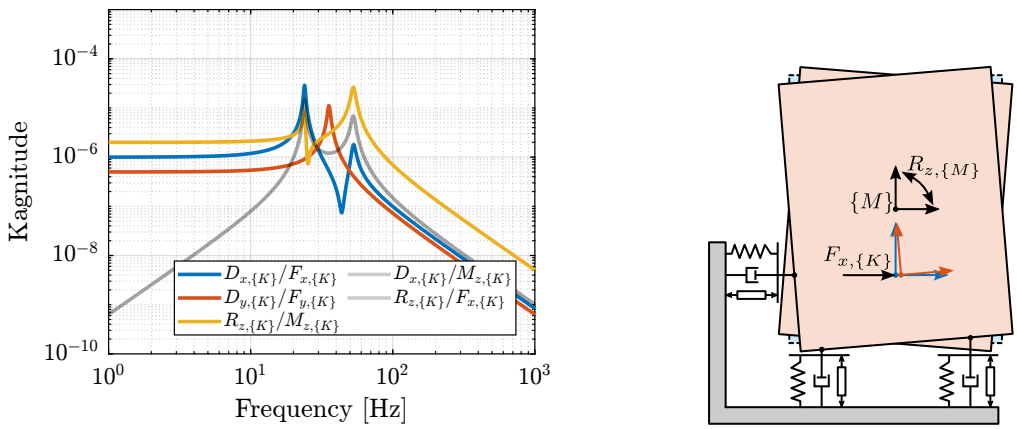


**(a)** Dynamics at the CoK

**(b)** High frequency force applied at the CoK

**Figure 2.5:** Plant decoupled using the Jacobian matrix expresssed at the center of stiffness (a). The physical reason for high frequency coupling is illustrated in (b).

## 2.4 Modal Decoupling

- A mechanical system consists of several modes:
  - Modal decomposition [51]

> he physical interpretation of the above two equations is that any motion of the system can be regarded as a combination of the contribution of the various modes.

  - Mode superposition [2], [52, chapt. 2]

- The idea is to control the system in the "modal space" [53] IFF in modal space [54] very interesting paper [5]

$$\boldsymbol{M}_{\{M\}}\ddot{\boldsymbol{\mathcal{X}}}_{\{M\}}(t) + \boldsymbol{C}_{\{M\}}\dot{\boldsymbol{\mathcal{X}}}_{\{M\}}(t) + \boldsymbol{K}_{\{M\}}\boldsymbol{\mathcal{X}}_{\{M\}}(t) = \boldsymbol{J}_{\{M\}}^{\mathsf{T}}\boldsymbol{\tau}(t) \tag{2.16}$$

Let's make a change of variables:

$$\boldsymbol{\mathcal{X}}_{\{M\}} = \boldsymbol{\Phi}\boldsymbol{\mathcal{X}}_m \tag{2.17}$$

with:

- $\boldsymbol{\mathcal{X}}_m$ the modal amplitudes
- $\boldsymbol{\Phi}$ a matrix whose columns are the modes shapes of the system which can be computed from $\boldsymbol{M}_{\{M\}}$ and $\boldsymbol{K}_{\{M\}}$.

By pre-multiplying the equation of motion (2.16) by $\boldsymbol{\Phi}^{\mathsf{T}}$ and using the change of variable (2.17), a new set of equation of motion are obtained

$$\underbrace{\boldsymbol{\Phi}^{\mathsf{T}}\boldsymbol{M}\boldsymbol{\Phi}}_{\boldsymbol{M}_m}\ddot{\boldsymbol{\mathcal{X}}}_m(t) + \underbrace{\boldsymbol{\Phi}^{\mathsf{T}}\boldsymbol{C}\boldsymbol{\Phi}}_{\boldsymbol{C}_m}\dot{\boldsymbol{\mathcal{X}}}_m(t) + \underbrace{\boldsymbol{\Phi}^{\mathsf{T}}\boldsymbol{K}\boldsymbol{\Phi}}_{\boldsymbol{K}_m}\boldsymbol{\mathcal{X}}_m(t) = \underbrace{\boldsymbol{\Phi}^{\mathsf{T}}\boldsymbol{J}^{\mathsf{T}}\boldsymbol{\tau}(t)}_{\boldsymbol{\tau}_m(t)} \tag{2.18}$$

- $\boldsymbol{\tau}_m$ is the modal input
- $\boldsymbol{M}_m$, $\boldsymbol{C}_m$ and $\boldsymbol{K}_m$ are the modal mass, damping and stiffness matrices

Orthogonality of normal modes gives that the "the modal vectors uncouple the equations of motion making each dynamic equation independent of all the others" [55]. The modal matrices are diagonal.

In order to implement such modal decoupling from the decentralized plant, architecture shown in Figure 2.6 can be used. The dynamics from modal inputs $\boldsymbol{\tau}_m$ to modal amplitudes $\boldsymbol{\mathcal{X}}_m$ is fully decoupled.

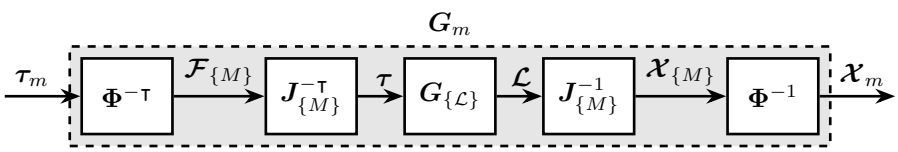


**Figure 2.6:** Modal Decoupling Architecture

Modal decoupling requires to have the equations of motion of the system. From the equations of motion (and more precisely the mass and stiffness matrices), the mode shapes $\Phi$ are computed.

Then, the system can be decoupled in the modal space. The obtained system on the diagonal are second order resonant systems which can be easily controlled.

Using this decoupling strategy, it is possible to control each mode individually.

- ☐ Do we need to measure all the states? I think so
- ☐ Say that the eigen vectors are unitary Are they orthogonal?
- ☐ Say that the obtained plant are second order systems

**Example** From the mass matrix $\boldsymbol{M}_{\{M\}}$ and stiffness matrix $\boldsymbol{K}_{\{M\}}$ expressed at the center of mass, the eigenvectors of $\boldsymbol{M}_{\{M\}}^{-1}\boldsymbol{K}_{\{M\}}$ are computed.

$$\boldsymbol{M}_{\{M\}} = \begin{bmatrix} m & 0 & 0 \\ 0 & m & 0 \\ 0 & 0 & I \end{bmatrix}, \quad \boldsymbol{K}_{\{M\}} = \begin{bmatrix} k & 0 & 0 \\ 0 & k & 0 \\ 0 & 0 & k \end{bmatrix} \tag{2.19}$$

Obtained

$$\boldsymbol{\Phi} = \begin{bmatrix} \frac{I-h_a^2 m-2l_a^2 m-\alpha}{2h_a m} & 0 & \frac{I-h_a^2 m-2l_a^2 m+\alpha}{2h_a m} \\ 0 & 1 & 0 \\ 1 & 0 & 1 \end{bmatrix}, \ \alpha = \sqrt{\left(I + m(h_a^2 - 2l_a^2)\right)^2 + 8m^2 h_a^2 l_a^2} \tag{2.20}$$

It may be very difficult to obtain eigenvectors analytically, so typically these can be computed numerically.

For the present test system, obtained eigen vectors are

Eigenvectors are arranged for increasing eigenvalues (i.e. resonance frequencies).

$$\boldsymbol{\phi} = \begin{bmatrix} -0.905 & 0 & -0.058 \\ 0 & 1 & 0 \\ 0.424 & 0 & -0.998 \end{bmatrix}, \quad \boldsymbol{\phi}^{-1} = \begin{bmatrix} -1.075 & 0 & 0.063 \\ 0 & 1 & 0 \\ -0.457 & 0 & -0.975 \end{bmatrix} \tag{2.21}$$

- ☐ Formula for the plant transfer function

## 2.5 SVD Decoupling

**Singular Value Decomposition** Singular Value Decomposition (SVD)

- Introduction to SVD [56, chapt. 1]
- Singular value is used a lot for multivariable control [43]. Used to study directions in multivariable systems.

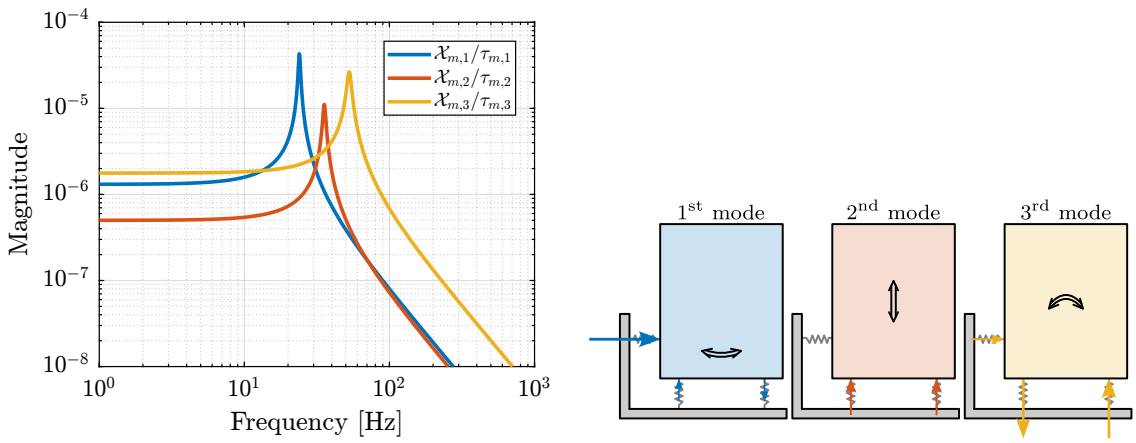


**(a)** Decoupled plant in modal space

**(b)** Individually controlled modes

**Figure 2.7:** Plant using modal decoupling consists of second order plants (a) which can be used to control separately different modes (b)

The SVD is a unique matrix decomposition that exists for every complex matrix $\boldsymbol{X} \in \mathbb{C}^{n\times m}$.

$$\boldsymbol{X} = \boldsymbol{U}\boldsymbol{\Sigma}\boldsymbol{V}^H \tag{2.22}$$

where $\boldsymbol{U} \in \mathbb{C}^{n\times n}$ and $\boldsymbol{V} \in \mathbb{C}^{m\times m}$ are unitary matrices with orthonormal columns, and $\boldsymbol{\Sigma} \in \mathbb{R}^{n\times n}$ is a diagonal matrix with real, non-negative entries on the diagonal.

If the matrix $\boldsymbol{X}$ is a real matrix, the obtained $\boldsymbol{U}$ and $\boldsymbol{V}$ matrices are real and can be used for decoupling purposes.

The idea to use Singular Value Decomposition as a way to decouple a plant is not new

- ☐ Quick review of SVD controllers [43, chapt. 3.5.4]

**Decoupling using the SVD** **Procedure**: Identify the dynamics of the system from inputs to outputs (can be obtained experimentally) Frequency Response Function, which is a complex matrix obtained for several frequency points $\boldsymbol{G}(\omega_i)$.

Choose a frequency where we want to decouple the system (usually, the crossover frequency $\omega_c$ is a good choice)

As *real* V and U matrices need to be obtained, a real approximation of the complex measured response needs to be computed. Compute a real approximation of the system's response at that frequency. [57]: real matrix that preserves the most orthogonality in directions with the input complex matrix

Then, a real matrix $\tilde{\boldsymbol{G}}(\omega_c)$ is obtained, and the SVD is performed on this real matrix. Unitary $\boldsymbol{U}$ and $\boldsymbol{V}$ matrices are then obtained such that $\boldsymbol{V}^{-\intercal}\tilde{\boldsymbol{G}}(\omega_c)\boldsymbol{U}^{-1}$ is diagonal.

Use the singular input and output matrices to decouple the system as shown in Figure 2.8

$$G_{\text{SVD}}(s) = \boldsymbol{U}^{-1}\boldsymbol{G}_{\{\mathcal{L}\}}(s)\boldsymbol{V}^{-\intercal} \tag{2.23}$$

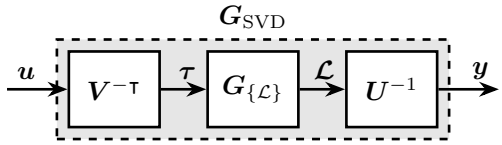


**Figure 2.8:** Decoupled plant $\boldsymbol{G}_{\text{SVD}}$ using the Singular Value Decomposition

In order to apply the Singular Value Decomposition, we need to have the Frequency Response Function of the system, at least near the frequency where we wish to decouple the system. The FRF can be experimentally obtained or based from a model.

This method ensure good decoupling near the chosen frequency, but no guaranteed decoupling away from this frequency.

Also, it depends on how good the real approximation of the FRF is, therefore it might be less good for plants with high damping.

This method is quite general and can be applied to any type of system. The inputs and outputs are ordered from higher gain to lower gain at the chosen frequency.

- ☐ Do we loose any physical meaning of the obtained inputs and outputs?
- ☐ Can we take advantage of the fact that U and V are unitary?

**Example**

$$\begin{aligned}
&\boldsymbol{G}_{\{\mathcal{L}\}}(\omega_c) = 10^{-9}\begin{bmatrix} -99-j2.6 & 74+j4.2 & -74-j4.2 \\ 74+j4.2 & -247-j9.7 & 102+j7.0 \\ -74-j4.2 & 102+j7.0 & -247-j9.7 \end{bmatrix} \\
&\xrightarrow[\text{approximation}]{\text{real}} \tilde{\boldsymbol{G}}_{\{\mathcal{L}\}(\omega_c)} = 10^{-9}\begin{bmatrix} -99 & 74 & -74 \\ 74 & -247 & 102 \\ -74 & 102 & -247 \end{bmatrix} \\
&\xrightarrow[\text{SVD}]{} \boldsymbol{U} = \begin{bmatrix} 0.34 & 0 & 0.94 \\ -0.66 & 0.71 & 0.24 \\ 0.66 & 0.71 & -0.24 \end{bmatrix}, \ \boldsymbol{V} = \begin{bmatrix} -0.34 & 0 & -0.94 \\ 0.66 & -0.71 & -0.24 \\ -0.66 & -0.71 & 0.24 \end{bmatrix}
\end{aligned} \tag{2.24}$$

Once the $\boldsymbol{U}$ and $\boldsymbol{V}$ matrices are obtained, the decoupled plant can be computed using (2.25).

$$\boldsymbol{G}_{\text{SVD}}(s) = \boldsymbol{U}^{-1}\boldsymbol{G}_{\{\mathcal{L}\}}(s)\boldsymbol{V}^{-\intercal} \tag{2.25}$$

The obtained plant shown in Figure 2.9 is very well decoupled. and not only around $\omega_c$. On top of that, the diagonal terms are second order plants.

- ☐ Do we have something special when applying SVD to a collocated MIMO system? As shown in Figure 2.2, the plant is symmetrical. Paper by Skogestad mention that. "symmetric circular plants" [58]

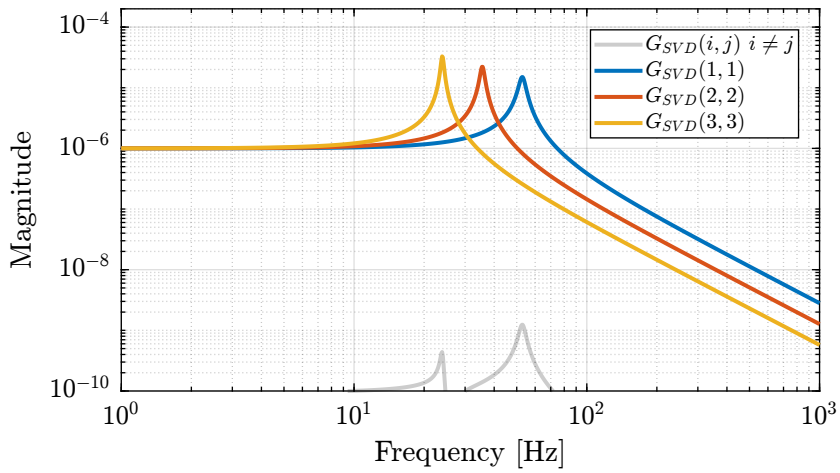


**Figure 2.9:** Svd plant $G_m(s)$

A second system, identical to the first in terms of dynamics. Just the sensor are changed. Instead of having relative motion sensors in the frame of the struts, three relative motion sensors are used as shown in Figure 2.10a. Using Jacobian matrices, it is possible to compute the relative motion of each struts. So theoretically, it should be possible to control both systems the same way.

However, when applying the same SVD decoupling, plant of Figure 2.10b is obtained. It has much more coupling. It is interesting to note that the coupling have local minimum near the chosen decoupling frequency. This is very logical as the decoupling matrices were computed from the plant response at that particular frequency.

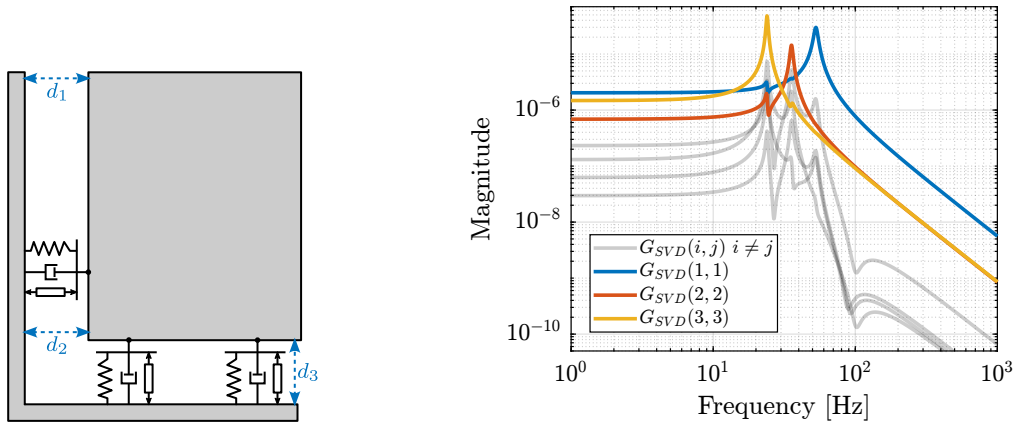


**(a)** Alternative location of sensors

**(b)** Obtained decoupled plant

**Figure 2.10:** Application of SVD decoupling on a system schematically shown in (a). The obtained decoupled plant is shown in (b).

## 2.6 Comparison of decoupling strategies

The three proposed methods may seem very similar as each of them consists of pre-multiplying and post-multiplying the plant with constant matrices. However, the three methods also differs by a number of points which are summarized in Table 2.3.

However, each method is quite different in terms of approach, and have different pros and cons.

- Comparison of the three proposed methods
- Different "approach" for the three methods:
  - Jacobian is based on geometry
  - Modal decoupling is based on dynamical equations
  - Singular Value Decoupling is based on measured frequency response function
- Depending on the decoupling method, the physical interpretation of inputs and outputs:
  - With Jacobian decoupling, the inputs and outputs can be easily interpreted physically. Inputs correspond to force/torques applied on a particular frames Outputs corresponds to translation and rotations expressed on a particular frame
  - With modal decoupling, inputs are arranged to excite individual modes. By doing a modal analysis (using a FEA for instance) it can be understood how actuator forces are combined to individually excite the different modes. Similarly, the outputs are combined to measure the different modes separately.
  - For singular value decomposition, inputs (resp. outputs) are special directions that are ordered from maximum to minimum controllability (resp. observability), at the chosen frequency. For plants such as parallel manipulators, it is difficult to have a physical interpretations of the decoupled plants inputs and outputs.
    - ☐ It is really linked to controllability? (add reference about that)
- Decoupling quality:
  - Jacobian: depending on the choice of frame, the plant may be well decoupled at low frequency (Center of Stiffness) or at high frequency (Center of Mass). If the system is designed to have both the CoK and the CoM at the same point, the use of Jacobian matrices may lead to excellent decoupling.
  - Modal: good decoupling is obtained for all frequencies. However, this is based on a model of the plant, and differences between the model and the physical implementation may lead to large off-diagonal elements. Diagonal elements are expected to be simple 2nd order low pass filters, which are easy to control.
  - SVD: as the decoupling matrices can be computed based on measured data, no model is required. Decoupling is expected to be good near the frequency chosen for computing the decoupling matrices, but may depend on how good the real approximation of the plant is for

that particular frequency. Whether the decoupling quality can be guaranteed away from the chosen frequency is unknown.

- "Frame" of the controllers: important to be able to tuned the controllers linked to performance metrics

There are other aspects that were not treated here such as:

- how to integrate feedforward path and reference signals

**Table 2.3:** Comparison of decoupling strategies

| | **Jacobian** | **Modal** | **SVD** |
|---|---|---|---|
| **Philosophy** | Topology Driven | Physics Driven | Data Driven |
| **Requirements** | Known geometry | Known equations of motion | Identified FRF |
| **Decoupling Matrices** | Decoupling using $\boldsymbol{J}_{\{O\}}$ obtained from geometry | Decoupling using $\boldsymbol{\Phi}$ obtained from modal decomposition | Decoupling using $\boldsymbol{U}$ and $\boldsymbol{V}$ obtained from SVD |
| **Decoupled Plant** | $\boldsymbol{G}_{\{O\}}(s) = \boldsymbol{J}_{\{O\}}^{-1}\boldsymbol{G}_{\mathcal{L}}(s)\boldsymbol{J}_{\{O\}}^{-\intercal}$ | $\boldsymbol{G}_m(s) = \boldsymbol{\Phi}^{-1}\boldsymbol{G}_{\mathcal{X}}(s)\boldsymbol{\Phi}^{-\intercal}$ | $\boldsymbol{G}_{\text{SVD}}(s) = \boldsymbol{U}^{-1}\boldsymbol{G}(s)\boldsymbol{V}^{-\intercal}$ |
| **Controller** | $\boldsymbol{K}_{\{O\}}(s) = \boldsymbol{J}_{\{O\}}^{-\intercal}\boldsymbol{K}_d(s)\boldsymbol{J}_{\{O\}}^{-1}$ | $\boldsymbol{K}_m(s) = \boldsymbol{\Phi}^{-\intercal}\boldsymbol{K}_d(s)\boldsymbol{\Phi}^{-1}$ | $\boldsymbol{K}_{\text{SVD}}(s) = \boldsymbol{V}^{-\intercal}\boldsymbol{K}_d(s)\boldsymbol{U}^{-1}$ |
| **Interpretation** | Forces/Torques to Displacement/Rotation in chosen frame | Inputs to excite individual modes<br><br>Output to sense individual modes | Directions of max to min controllability/observability |
| **Properties** | Decoupling at low or high frequency depending on the chosen frame | Good decoupling at all frequencies | Good decoupling near the chosen frequency |
| **Pros** | Physical inputs / outputs<br><br>Good decoupling at High frequency (diagonal mass matrix if Jacobian taken at the CoM)<br>Good decoupling at Low frequency (if Jacobian taken at specific point)<br>Easy integration of meaningful reference inputs | Target specific modes<br><br>2nd order diagonal plant | Good Decoupling near the crossover<br>Very General |
| **Cons** | Coupling between force/rotation may be high at low frequency (non diagonal terms in K)<br>Limited to parallel mechanisms (?)<br>If good decoupling at all frequencies =¿ requires specific mechanical architecture | Need analytical equations | Loose the physical meaning of inputs /outputs<br><br>Decoupling depends on the real approximation validity<br>Diagonal plants may not be easy to control |
| **Applicability** | Parallel Mechanisms<br><br>Only small motion for the Jacobian matrix to stay constant | Systems whose dynamics that can be expressed with M and K matrices | Very general<br><br>Need FRF data (either experimentally or analytically) |

Conclusion about NASS:

- Prefer to use Jacobian decoupling as we get more physical interpretation

- Also, it is possible to take into account different specifications in the different DoF as the control is in a "frame" which corresponds to the specifications. For active damping however, it may be reasonable to work in the modal space as different damping may be applied to different modes [54].

# 3 Closed-Loop Shaping using Complementary Filters

Once the system is properly decoupled using one of the approaches described in Section 2, a diagonal controller can be tuned. This consists in tuning several SISO controllers. There are several ways to design a controller to obtain a given performance while ensuring good robustness properties.

Performances of a feedback system (such as response time, disturbance rejection, ) depends on the obtained closed-loop transfer functions. For instance sensitivity, transmissibility, etc... Gang of Four. The specifications can usually be expressed in terms of the shape of these closed-loop transfer functions [43, chapt. 3].

In some cases, "fixed" controller structures are used, with as PI and PID controllers. In such case the controller coefficients are manually tuned to obtain acceptable performance and robustness. In many cases, PID+LPF can already lead to performances close to optimal, depending on the plant.

Decoupled Open-Loop Shaping:

- Explain procedure when applying open-loop shaping **schmidt20˙desig˙high˙perfor˙mechat˙third˙revis˙edition steinbuch16˙model˙based**

  > he key idea of loop-shaping is the modification of the controller such that the open- loop is made according to specifications. The reason this works so well, is that the controller enters linearly into the open-loop transfer l(j!) = g(j!)k(j!), so that it is fast and easy to reason what is to be changed in the controller. However, in practice all specifications are of course given in terms of the final system performance, i.e. as closed-loop specifications. So we should convert the closed loop specs into specs on the open-loop.

- The controller is usually manually tuned using a series of Integrators, Leads, Lags, Notches, low pass filters

- There are lots of tools to check stability, robustness margins and performances

- Open-Loop shaping is very popular as the open-loop gain depends linearly on the controller. So the open-loop transfer function can easily be shaped by modifying the controller response.

- Different techniques for open loop shaping (choice of optimal open-loop gain shape) [60]

- But this is open-loop shaping, and it does not directly work on the closed loop transfer functions

- The huge advantage of this technique, is that one can tune the controllers based on the measured FRF of the system. No plant model is required.

- This is what was done during the conceptual phase after the plan was decoupled in the frame of the struts.

Model based control:

- Review of model based design (LQG, H-Infinity) applied to Stewart platform Multivariable Control loop-shaping [43].
- Difficulty to specify robustness to change of payload mass
- Requires high level of expertise. Far from standard in industry. Application to Stewart platforms is not demonstrated (or performance increased compared to decoupled control and manual loop shaping).

In this section, an alternative controller synthesis scheme is proposed in which complementary filters are used for directly shaping the closed-loop transfer functions. In this paper, we propose a new controller synthesis method

- based on the use of complementary high pass and low pass filters
- inverse based control
- direct translation of requirements such as disturbance rejection and robustness to plant uncertainty

## 3.1 Control Architecture

**Virtual Sensor Fusion** Let's consider the control architecture represented in Figure 3.1 where $G'$ is the physical plant to control, $G$ is a model of the plant, $k$ is a gain, $H_L$ and $H_H$ are complementary filters ($H_L(s) + H_H(s) = 1$). The signals are the reference signal $r$, the output perturbation $d_y$, the measurement noise $n$ and the control input $u$.

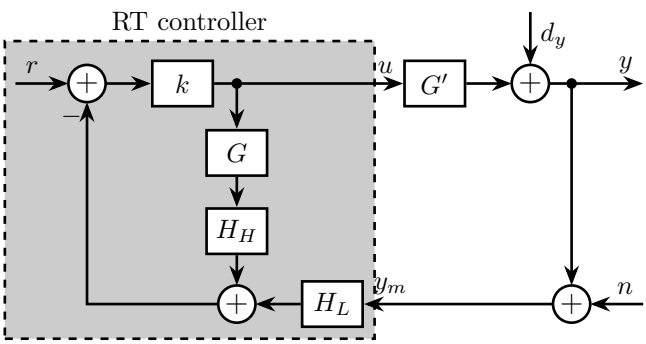


**Figure 3.1:** Sensor Fusion Architecture

The dynamics of the closed-loop system is described by (3.1) with $L = k(GH_H + G'H_L)$.

$$y = \frac{1 + kGH_H}{1 + L} dy + \frac{kG'}{1 + L} r - \frac{kG'H_L}{1 + L} n \tag{3.1a}$$

$$u = -\frac{kH_L}{1 + L} dy \quad + \frac{k}{1 + L} r - \frac{kH_L}{1 + L} n \tag{3.1b}$$

The idea of using such architecture comes from sensor fusion [26], [61] where two sensors are used. One is measuring the quantity that is required to control, the other is collocated with the actuator in such a way that stability is guaranteed. The first one is low pass filtered in order to obtain good performance at low frequencies and the second one is high pass filtered to benefits from its good dynamical properties.

Here, the second sensor is replaced by a model $G$ of the plant which is assumed to be stable and minimum phase. This lead to the idea of virtual sensor fusion presented in **verma20˙virtual˙sensor˙fusion˙high˙precis˙contr**.

One may think that the control architecture shown in Figure 3.1 is a multi-loop system, but because no non-linear saturation-type element is present in the inner-loop (containing $k$, $G$ and $H_H$ which are all numerically implemented), the structure is equivalent to the architecture shown in Figure 3.2.

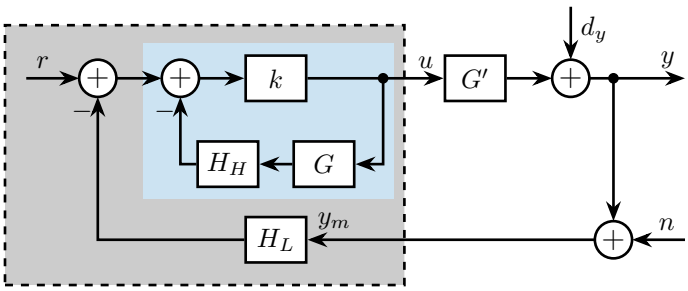


**Figure 3.2:** Equivalent feedback architecture

The dynamics of the system can be rewritten (3.2) with $K = \frac{k}{1+H_H Gk}$.

$$y = \frac{1}{1 + G'KH_L} dy + \frac{G'K}{1 + G'KH_L} r - \frac{G'KH_L}{1 + G'KH_L} n \tag{3.2a}$$

$$u = \frac{-KH_L}{1 + G'KH_L} dy + \frac{K}{1 + G'KH_L} r - \frac{KH_L}{1 + G'KH_L} n \tag{3.2b}$$

**Asymptotic behavior** Let's take the extreme case of very high values for $k$. In that case $K(s)$ converges to plant inverse multiply by the inverse of the high pass filter (3.3).

$$\lim_{k \to \infty} K(s) = \lim_{k \to \infty} \frac{k}{1 + H_H(s)G(s)k} = (H_H(s)G(s))^{-1} \tag{3.3}$$

If the obtained $K$ is improper, a low pass filter can be added to have its causal realization. Also, we want $K$ to be stable, so $G$ and $H_H$ must be minimum phase transfer functions.

With this assumptions, the resulting control architecture is shown on Figure 3.3. The only "tuning parameters" are the complementary filters $H_L$ and $H_H$.

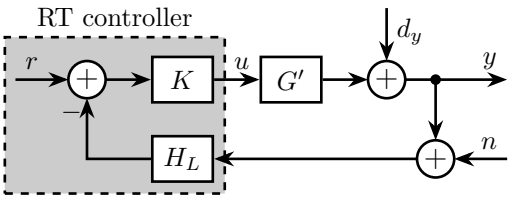


**Figure 3.3:** Equivalent classical feedback control architecture

The equations describing the dynamics of the closed-loop system of Figure 3.3

$$y = \frac{H_H dy + G'G^{-1}r - G'G^{-1}H_L n}{H_H + G'G^{-1}H_L} \tag{3.4a}$$

$$u = \frac{-G^{-1}H_L dy + G^{-1}r - G^{-1}H_L n}{H_H + G'G^{-1}H_L} \tag{3.4b}$$

At frequencies where the model is accurate: $G^{-1}G' \approx 1$, $H_H + G'G^{-1}H_L \approx H_H + H_L = 1$ and the closed loop transfer functions are described by (3.5).

$$y = H_H dy \qquad + r \qquad - H_L n \tag{3.5a}$$

$$u = -G^{-1}H_L dy + G^{-1}r - G^{-1}H_L n \tag{3.5b}$$

The obtained sensitivity transfer function equals to the high pass filter $S = \frac{y}{dy} = H_H$ and the transmissibility transfer function equals to the low pass filter $T = \frac{y}{n} = H_L$.

Assuming that we have a good model of the plant, we have then that the closed-loop behavior of the system converges to the designed complementary filters.

## 3.2 Translating the performance requirements into the shapes of the complementary filters

The required performance specifications in a feedback system can usually be translated into requirements on the upper bounds of $|S(j\omega)|$ and $|T(j\omega)|$ [62]. The process of designing a controller $K(s)$ in order to obtain the desired shapes of $|S(j\omega)|$ and $|T(j\omega)|$ is called closed-loop shaping.

The equations (3.4a) and (3.4b) describing the dynamics of the studied feedback architecture are not written in terms of the controller $K(s)$ but in terms of the complementary filters $H_L(s)$ and $H_H(s)$. The typical specifications are then translated into the desired shapes of the complementary filters.

**Nominal Stability (NS)** The closed-loop system is stable if all its elements are stable ($K$, $G'$ and $H_L$) and if the sensitivity function ($S = \frac{1}{1+G'KH_L}$) is stable. For the nominal system ($G' = G$), the sensitivity transfer function is equal to the high pass filter: $S(s) = H_H(s)$.

Nominal stability is then guaranteed if $H_L$, $H_H$ and $G$ are stable and if $G$ and $H_H$ are minimum phase (to have $K$ stable). Therefore stable and minimum phase complementary filters need to be used.

**Nominal Performance (NP)** Two performance weights $w_H$ and $w_L$ are here defined in such a way that performance specifications are satisfied is (3.6) is satisfied.

$$|w_H(j\omega)S(j\omega)| \leq 1 \quad \forall\omega \tag{3.6a}$$
$$|w_L(j\omega)T(j\omega)| \leq 1 \quad \forall\omega \tag{3.6b}$$

For the nominal system, we have $S = H_H$ and $T = H_L$, and then nominal performance is ensured by requiring (**??**).

$$\boxed{\text{NP} \iff \begin{cases} |w_H(j\omega)H_H(j\omega)| \leq 1 & \forall\omega \\ |w_L(j\omega)H_L(j\omega)| \leq 1 & \forall\omega \end{cases}} \tag{3.7, 3.8}$$

The translation of typical performance requirements on the shapes of the complementary filters is discussed below:

- for disturbance rejections, make $|S| = |H_H|$ small
- for noise attenuation, make $|T| = |H_L|$ small
- closed-loop bandwidth can be limited by requiring that $|T|$ is less than $\frac{1}{\sqrt{2}}$ above the maximum wanted bandwidth

Therefore, by properly choosing the shape of the complementary filters, the nominal performance specifications can be addressed.

Classical stability margins (gain and phase margins) can also be linked to the maximum amplitude of the sensitivity transfer function.

☐ Add reference

Typically, having $|S|_\infty \leq 2$ guarantees a gain margin of at least 2 and a phase margin of at least 29°.

**Response time to change of reference signal** For the nominal system, the model is accurate and the transfer function from reference signal $r$ to output $y$ is 1 (3.5a) and does not depends of the complementary filters.

However, one can add a pre-filter as shown in Figure 3.4.

The transfer function from $y$ to $r$ becomes $\frac{y}{r} = K_r$ and $K_r$ can we chosen to obtain acceptable response to change of the reference signal. Typically, $K_r$ is a low pass filter of the form

$$K_r(s) = \frac{1}{1 + \tau s} \tag{3.9}$$

with $\tau$ corresponding to the desired response time.

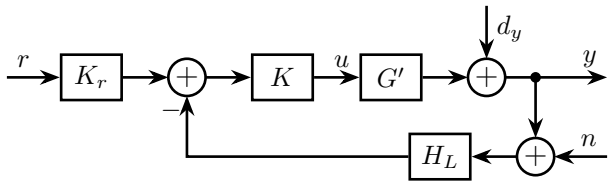


**Figure 3.4:** Prefilter used to limit input usage

**Input usage** Input usage due to disturbances $d_y$ and measurement noise $n$ is determined by $\left|\frac{u}{d_y}\right| = \left|\frac{u}{n}\right| = \left|G^{-1}H_L\right|$. Thus it can be limited by setting an upper bound on $|H_L|$.

Input usage due to reference signal $r$ is determined by $\left|\frac{u}{r}\right| = \left|G^{-1}K_r\right|$ when using a pre-filter (Figure 3.4) and $\left|\frac{u}{r}\right| = \left|G^{-1}\right|$ otherwise.

Proper choice of $|K_r|$ is then useful to limit input usage due to change of reference signal.

**Robust Stability (RS)** Robustness stability represents the ability of the control system to remain stable even though there are differences between the actual system $G'$ and the model $G$ that was used for the design of the controller. These differences can have various origins such as unmodelled dynamics or non-linearities.

To represent the differences between the model and the actual system, the input multiplicative uncertainty as represented in Figure 3.5a is used.

Then, the set of possible plant is described by (3.10). $w_I$ should be chosen such that all possible plants $G'$ are contained in the set $\Pi_i$.

$$\Pi_i : \quad G'(s) = G(s)\big(1 + w_I(s)\Delta_I(s)\big); \quad |\Delta_I(j\omega)| \leq 1 \ \forall\omega \tag{3.10}$$

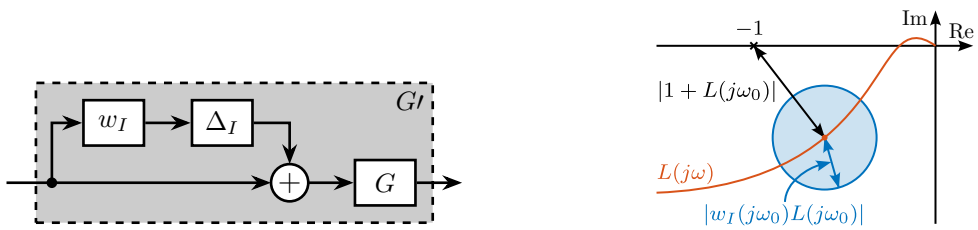


**(a)** Input multiplicative uncertainty **(b)** Nyquist plot - Effect of multiplicative uncertainty

**Figure 3.5:** Input multiplicative uncertainty to model the differences between the model and the physical plant (a). Effect of this uncertainty is displayed on the Nyquist plot (b)

Considering input multiplicative uncertainty, the robust stability property can be derived graphically from the Nyquist plot (Figure 3.5b), and (3.11) is obtained, as proposed in [43, chapt. 7.5.1].

$$\text{RS} \iff |w_I(j\omega)L(j\omega)| \leq |1 + L(j\omega)| \quad \forall\omega \tag{3.11}$$

After some algebraic manipulations, robust stability is then guaranteed by having the low pass filter $H_L$ satisfying (3.12).

$$\boxed{\text{RS} \iff |w_I(j\omega)H_L(j\omega)| \leq 1 \quad \forall\omega} \tag{3.12}$$

**Robust Performance (RP)** Robust performance is a property for a controlled system to have its performance guaranteed even though the dynamics of the plant is changing within specified bounds.

For robust performance, we then require to have the performance condition valid for all possible plants in the defined uncertainty set (3.13).

$$\text{RP} \iff |w_H(j\omega)S(j\omega)| \leq 1 \quad \forall G' \in \Pi_I,\ \forall\omega \tag{3.13}$$

Let's transform condition (3.13) into a condition on the complementary filters (3.14).

$$\boxed{\text{RP} \iff |w_H(j\omega)H_H(j\omega)| + |w_I(j\omega)H_L(j\omega)| \leq 1,\ \forall\omega} \tag{3.14}$$

Obtained condition for robust performance combines both the NP and RS conditions. If both NP and RS conditions are fulfilled, the robust performance will be fulfilled with a factor 2 [43, chapt. 7.6]. Therefore, for SISO systems, robust stability and nominal performance are usually sufficient.

## 3.3 Complementary filter design

As was explained in Section 1, complementary filters can easily be shaped with the standard $\mathcal{H}_\infty$ synthesis. As requirements can usually be expressed as upper bounds on the complementary filters' magnitude, this method is very well suited.

However, analytical formulas for complementary filters may also be used.

For some applications, first order complementary filters (3.15) are sufficient.

$$H_L(s) = \frac{1}{1 + s/\omega_0} \tag{3.15a}$$

$$H_H(s) = \frac{s/\omega_0}{1 + s/\omega_0} \tag{3.15b}$$

They can be expressed analytically in the digital domain using the Bilinear transformation. In such case, digital filters (3.16) are obtained.

$$H_L(z^{-1}) = \frac{T_s\omega_0 + T_s\omega_0 z^{-1}}{T_s\omega_0 + 2 + (T_s\omega_0 - 2)z^{-1}} \tag{3.16a}$$

$$H_H(z^{-1}) = \frac{2 - 2z^{-1}}{T_s\omega_0 + 2 + (T_s\omega_0 - 2)z^{-1}} \tag{3.16b}$$

The main advantage of having analytical formulas for the complementary filters is that the parameter $\omega_0$ may be modified in real time. This is illustrated in Figure 3.6. Therefore, the performance and robustness of different control bandwidth can be tested very quickly.

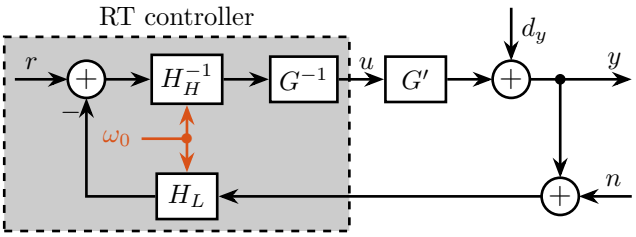


**Figure 3.6:** Implemented digital complementary filters with parameter $\omega_0$ that can be changed in real time

For many applications, slope of $+2$ is wanted at low frequency for the sensitivity transfer function (to follow ramp inputs for instance), and a slope of $-2$ for the complementary sensitivity transfer function. In that case, complementary filters shown in equation (3.17) are proposed.

$$H_L(s) = \frac{(1+\alpha)(\frac{s}{\omega_0}) + 1}{\left((\frac{s}{\omega_0}) + 1\right)\left((\frac{s}{\omega_0})^2 + \alpha(\frac{s}{\omega_0}) + 1\right)} \tag{3.17a}$$

$$H_H(s) = \frac{(\frac{s}{\omega_0})^2\left((\frac{s}{\omega_0}) + 1 + \alpha\right)}{\left((\frac{s}{\omega_0}) + 1\right)\left((\frac{s}{\omega_0})^2 + \alpha(\frac{s}{\omega_0}) + 1\right)} \tag{3.17b}$$

The effect of $\alpha$ and $\omega_0$ and the obtained shape of the complementary filters is shown in Figure 3.7. Such filters can also be implemented in the digital domain with analytical formulas, such as $\alpha$ and $\omega_0$ can be changed in real time.

## 3.4 Numerical Example

**Procedure** In order to apply this control technique, we propose the following procedure:

1. Identify the plant to be controlled in order to obtain the plant model $G$
2. Design the weighting function $w_I$ such that all possible plants $G'$ are contained in the set $\Pi_i$
3. Translate the performance requirements into upper bounds on the complementary filters (as explained in Section 3.2)

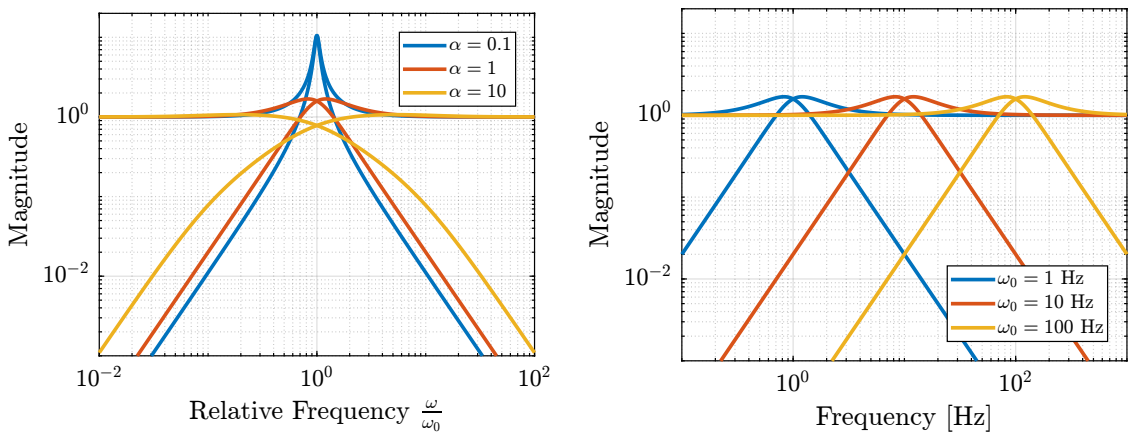


**(a)** Effect of $\alpha$

**(b)** Effect of $\omega_0$

**Figure 3.7:** Shape of proposed analytical complementary filters. Effect of $\alpha$ (a) and $\omega_0$ (b) are shown.

4. Design the weighting functions $w_H$ and $w_L$ and generate the complementary filters using $\mathcal{H}_\infty$-synthesis (as was explained in Section 1.3). If the synthesis fails to give filters satisfying the upper bounds previously defined, either the requirements have to be reworked or a better model $G$ that will permits to have a smaller $w_I$ should be obtained. For simple cases, analytical formulas of complementary filters given in Section 3.3 can be used.

5. If $K(s) = (G(s)H_H(s))^{-1}$ is not proper, low pass filters should be added high a high corner frequency

### Plant

- To test this control architecture, a simple test model is used (Figure 3.8a).

- This model is quite similar to many positioning stages for Synchrotrons. A payload (i.e. sample) with mass $m = 5$ is positioned on top of the stage. The goal is to position the sample with respect to the x-ray. It is supposed that the relative position $y$ between the payload an the x-ray is measured (typically the relative position between the focusing optics and the sample is performed). There are some disturbance forces acting on the positioning stability, such as stage vibration $d_w$ and direct forces applied on the sample $d_F$ (for instance cable forces). The positioning stage itself has a stiffness $k$, an internal damping $c$ and the force $F$ can be controlled.

The model of the plant $G(s)$ from actuator force $F$ to displacement $y$ is then

$$G(s) = \frac{1}{ms^2 + cs + k} \tag{3.18}$$

The values for the parameters of the models are $m = 20\,\text{kg}$, $k = 1\text{N}/\mu\text{m}$ and $c = 10^2\text{N}/(\text{m/s})$.

The plant dynamics has some uncertainty related to the limited support compliance, unmodeled flexible dynamics, dynamics of the payload, etc. A multiplicative input uncertainty weight $w_I(s)$ is used to specify the amount of uncertainty as a function of frequency (3.19).

$$w_I(s) = 10 \cdot \frac{(s+100)^2}{(s+1000)^2} \tag{3.19}$$

The nominal plant dynamics as well as the entire set of possible plants $\Pi_i$ are shown in Figure 3.8b.

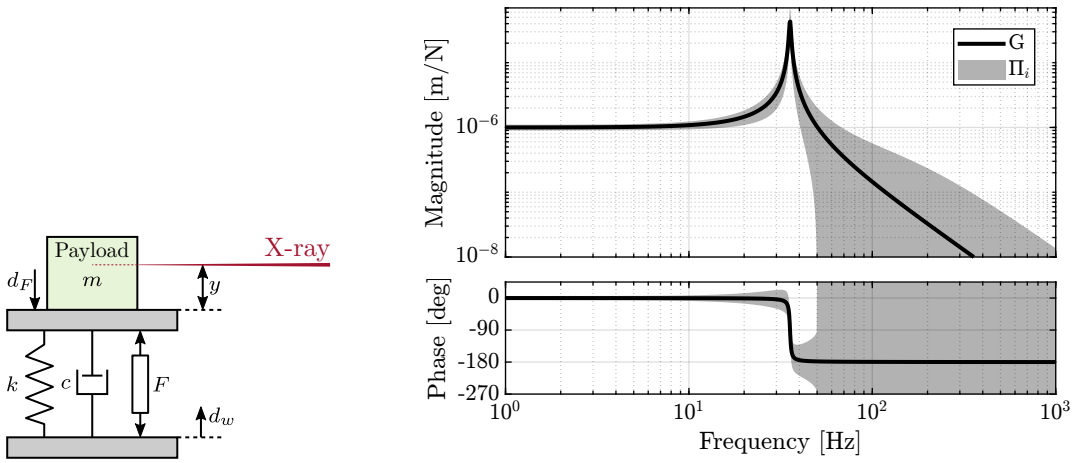


**(a)** Test model

**(b)** Bode plot of $G(s)$ and associated uncertainty set

**Figure 3.8:** Schematic of the test system (a). Bode plot of the transfer function $G(s)$ from $F$ to $y$ and the associated uncertainty set (b).

**Requirements and choice of complementary filters** As explained in Section 3.2, nominal performance requirements can be expressed as upper bounds on the complementary filter shapes.

- Be able to follow ramp inputs (i.e. constant velocity scans) with no steady-state tracking error. This requires to have a +2 slope at low frequency for $|S(j\omega)|$
- Filter the measurement noise above 300Hz as the sensor noise is high (say a filtering factor of 100 is needed above that frequency).
- As much disturbance rejection as possible.

The second requirement is to have robust stability meaning that the plant should remain stable while considering the dynamical uncertainties modelled with $w_I$

- The low-pass complementary filter magnitude $|H_L(j\omega)|$ should be bellow the inverse magnitude of the uncertainty weight magnitude $|w_I(j\omega)|$ (3.12)

Robust performance is ensured by simultaneous NP and RS.

All the requirements on $H_L$ and $H_H$ are represented on Figure 3.9a.

While the $\mathcal{H}_\infty$ synthesis of complementary filters could be used, for this simple examples with simple requirements, analytical formulas of complementary filters were used.

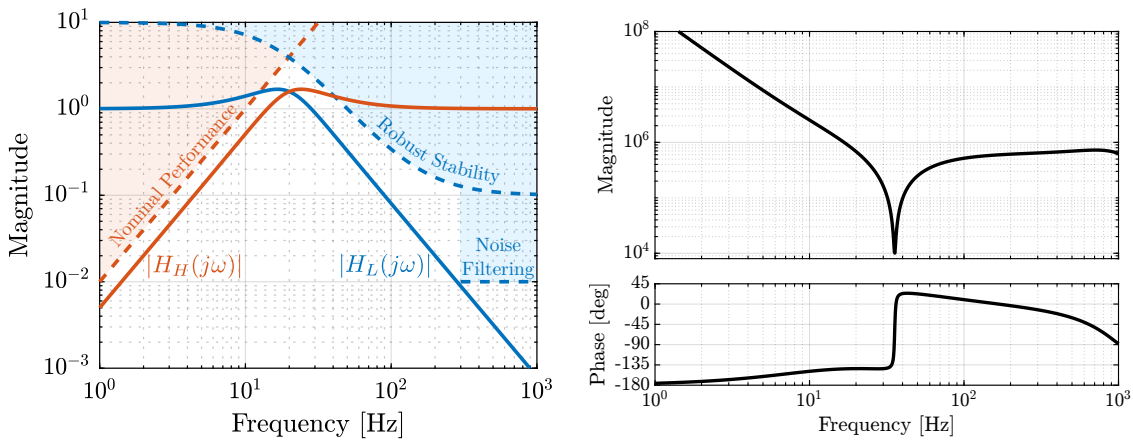


**(a)** Specifications and complementary filters

**(b)** Bode plot of $K(s) \cdot H_L(s)$

**Figure 3.9:** Performance requirement and complementary filters used (a). Obtained controller from the complementary filters and the plant inverse is shown in (b).

For this simple example, analytical formulas proposed to have +2 and -2 slopes (3.17) were used. $\alpha = 1$ and $\omega_0 = 2\pi \cdot 20$ were used.

**Controller analysis** The controller to be implemented is $K(s) = \tilde{G}^{-1}(s)H_H^{-1}(s)$, with $\tilde{G}^{-1}(s)$ is the plant inverse which needs to be stable and proper. Therefore, some low pass filters are added at high frequency (3.20).

$$\tilde{G}^{-1}(s) = \frac{ms^2 + cs + k}{1 + \frac{s}{2\pi \cdot 1000} + \left(\frac{s}{2\pi \cdot 1000}\right)^2} \tag{3.20}$$

The obtained bode plot of the controller times the complementary high pass filter is shown in Figure 3.9b.

- two integrators are present at low frequency to be able to follow ramp inputs
- a notch is located at the plant resonance (inverse)
- a lead is added near the bandwidth around 20 Hz

**Robustness and Performance analysis** The robust stability can be access on the Nyquist plot (Figure 3.10a). Even when considering all the possible plants in the uncertainty set, the nyquist plot stays away from the unstable point, indicating good robustness.

The performance is evaluated by looking at the closed-loop sensitivity and complementary sensitivity transfer functions (Figure 3.10b).

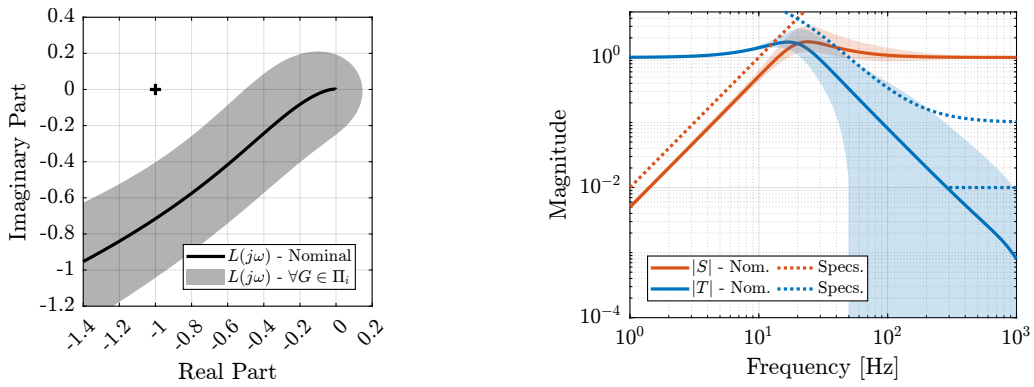


**(a)** Robust Stability

**(b)** Nominal and Robust performance

**Figure 3.10:** Validation of Robust stability with the Nyquist plot (a) and validation of the nominal and robust performance with the magnitude of the closed-loop transfer functions (b)

## Conclusion

- ☐ Say that the presented control architecture in this section No ambition to overcome fundamental limitations of current architectures. Very similar to Internal Model Control **saxena12˙advan˙inter˙model˙contr˙t** Had no time to proceed to an extensive literature review to find similar control architecture and to compare them. Whether the propose architecture has advantages compared to already excising architecture in the literature is not clear.

- ☐ The control architecture was presented for a SISO system, but can be applied to MIMO if decoupling is sufficient. It will be experimentally demonstrated with the NASS.

- ☐ Discuss how useful it is as the bandwidth can be changed in real time with analytical formulas of second order complementary filters. Maybe make a section about that. Maybe give analytical formulas of second order complementary filters in the digital domain?

- ☐ Disadvantages:
  - not optimal
  - computationally intensive?
  - lead to inverse control which may not be wanted in many cases. Add reference.

# Conclusion

# Bibliography


[1] Z. J. Geng, G. G. Pan, L. S. Haynes, B. K. Wada, and J. A. Garba, "An intelligent control system for multiple degree-of-freedom vibration isolation," *Journal of Intelligent Material Systems and Structures*, vol. 6, no. 6, pp. 787–800, 1995 (cit. on pp. 4, 5).

[2] A. Preumont, *Vibration Control of Active Structures - Fourth Edition* (Solid Mechanics and Its Applications). Springer International Publishing, 2018 (cit. on pp. 4, 25).

[3] C. Wang, X. Xie, Y. Chen, and Z. Zhang, "Investigation on active vibration isolation of a stewart platform with piezoelectric actuators," *Journal of Sound and Vibration*, vol. 383, pp. 1–19, Nov. 2016 (cit. on pp. 4, 5).

[4] X. Li, J. C. Hamann, and J. E. McInroy, "Simultaneous vibration isolation and pointing control of flexure jointed hexapods," in *Smart Structures and Materials 2001: Smart Structures and Integrated Systems*, Aug. 2001 (cit. on pp. 4, 5, 18).

[5] H. Pu, X. Chen, Z. Zhou, and X. Luo, "Six-degree-of-freedom active vibration isolation system with decoupled collocated control," *Proceedings of the Institution of Mechanical Engineers, Part B: Journal of Engineering Manufacture*, vol. 226, no. 2, pp. 313–325, 2011 (cit. on pp. 4, 5, 18, 25).

[6] X. Xie, C. Wang, and Z. Zhang, "Modeling and control of a hybrid passive/active stewart vibration isolation platform," in *INTER-NOISE and NOISE-CON Congress and Conference Proceedings*, Institute of Noise Control Engineering, vol. 255, 2017, pp. 1844–1853 (cit. on pp. 4, 5, 18).

[7] D. Tjepkema, "Active hard mount vibration isolation for precision equipment [ph. d. thesis]," Ph.D. dissertation, 2012 (cit. on pp. 4, 5).

[8] D. Tjepkema, J. van Dijk, and H. Soemers, "Sensor fusion for active vibration isolation in precision equipment," *Journal of Sound and Vibration*, vol. 331, no. 4, pp. 735–749, 2012 (cit. on pp. 4–6).

[9] G. Hauge and M. Campbell, "Sensors and control of a space-based six-axis vibration isolation system," *Journal of Sound and Vibration*, vol. 269, no. 3-5, pp. 913–931, 2004 (cit. on pp. 4, 5).

[10] M. A. Beijen, D. Tjepkema, and J. van Dijk, "Two-sensor control in active vibration isolation using hard mounts," *Control Engineering Practice*, vol. 26, pp. 82–90, 2014 (cit. on p. 4).

[11] Y. K. Yong and A. J. Fleming, "High-speed vertical positioning stage with integrated dual-sensor arrangement," *Sensors and Actuators A: Physical*, vol. 248, pp. 184–192, 2016 (cit. on pp. 4, 6, 7).

[12] X. Yang, H. Wu, B. Chen, S. Kang, and S. Cheng, "Dynamic modeling and decoupled control of a flexible stewart platform for vibration isolation," *Journal of Sound and Vibration*, vol. 439, pp. 398–412, Jan. 2019 (cit. on pp. 5, 18).

[13] D. Thayer and J. Vagners, "A look at the pole/zero structure of a stewart platform using special coordinate basis," in *Proceedings of the 1998 American Control Conference. ACC (IEEE Cat. No.98CH36207)*, 1998 (cit. on p. 5).

[14] D. Thayer, M. Campbell, J. Vagners, and A. von Flotow, "Six-axis vibration isolation system using soft actuators and multiple sensors," *Journal of Spacecraft and Rockets*, vol. 39, no. 2, pp. 206–212, 2002 (cit. on pp. 5, 18).

[15] J. McInroy, "Dynamic modeling of flexure jointed hexapods for control purposes," in *Proceedings of the 1999 IEEE International Conference on Control Applications (Cat. No.99CH36328)*, 1999 (cit. on pp. 5, 18).

[16] J. McInroy, J. O'Brien, and G. Neat, "Precise, fault-tolerant pointing using a stewart platform," *IEEE/ASME Transactions on Mechatronics*, vol. 4, no. 1, pp. 91–95, 1999 (cit. on pp. 5, 18).

[17] J. McInroy and J. Hamann, "Design and control of flexure jointed hexapods," *IEEE Transactions on Robotics and Automation*, vol. 16, no. 4, pp. 372–381, 2000 (cit. on pp. 5, 18).

[18] J. Bendat, "Optimum filters for independent measurements of two related perturbed messages," *IRE Transactions on Circuit Theory*, 1957 (cit. on p. 6).

[19] F. Shaw and K. Srinivasan, "Bandwidth enhancement of position measurements using measured acceleration," *Mechanical Systems and Signal Processing*, vol. 4, no. 1, pp. 23–38, 1990 (cit. on pp. 6, 7).

[20] M. Zimmermann and W. Sulzer, "High bandwidth orientation measurement and control based on complementary filtering," *Robot Control 1991*, Robot Control 1991, pp. 525–530, 1992 (cit. on pp. 6, 7).

[21] H. G. Min and E. T. Jeung, "Complementary filter design for angle estimation using mems accelerometer and gyroscope," *Department of Control and Instrumentation, Changwon National University, Changwon, Korea*, pp. 641–773, 2015 (cit. on pp. 6, 7).

[22] W. Hua, "Low frequency vibration isolation and alignment system for advanced ligo," Ph.D. dissertation, stanford university, 2005 (cit. on pp. 6, 7).

[23] W. Hua, D. B. Debra, C. T. Hardham, B. T. Lantz, and J. A. Giaime, "Polyphase fir complementary filters for control systems," in *Proceedings of ASPE Spring Topical Meeting on Control of Precision Systems*, 2004, pp. 109–114 (cit. on pp. 6, 7).

[24] A. R. Plummer, "Optimal complementary filters and their application in motion measurement," *Proceedings of the Institution of Mechanical Engineers, Part I: Journal of Systems and Control Engineering*, vol. 220, no. 6, pp. 489–507, 2006 (cit. on pp. 6, 7).

[25] P. Y. C. H. Robert Grover Brown, *Introduction to Random Signals and Applied Kalman Filtering with Matlab Exercises*, 4th ed. Wiley, 2012 (cit. on p. 6).

[26] C. Collette and F. Matichard, "Sensor fusion methods for high performance active vibration isolation systems," *Journal of Sound and Vibration*, vol. 342, pp. 1–21, 2015 (cit. on pp. 6, 7, 35).

[27] A.-J. Baerveldt and R. Klang, "A low-cost and low-weight attitude estimation system for an autonomous helicopter," in *Proceedings of IEEE International Conference on Intelligent Engineering Systems*, 1997 (cit. on pp. 6, 7).

[28] P. Corke, "An inertial and visual sensing system for a small autonomous helicopter," *Journal of Robotic Systems*, vol. 21, no. 2, pp. 43–51, 2004 (cit. on pp. 6, 7).

[29] A. Jensen, C. Coopmans, and Y. Chen, "Basics and guidelines of complementary filters for small uas navigation," in *2013 International Conference on Unmanned Aircraft Systems (ICUAS)*, May 2013 (cit. on pp. 6, 7).

[30] A. Pascoal, I. Kaminer, and P. Oliveira, "Navigation system design using time-varying complementary filters," in *Guidance, Navigation, and Control Conference and Exhibit*, 1999 (cit. on pp. 6, 7).

[31] P. Batista, C. Silvestre, and P. Oliveira, "Optimal position and velocity navigation filters for autonomous vehicles," *Automatica*, vol. 46, no. 4, pp. 767–774, 2010 (cit. on p. 6).

[32] J. van Heijningen, "Low-frequency performance improvement of seismic attenuation systems and vibration sensors for next generation gravitational wave detectors," Ph.D. dissertation, Vrije Universiteit, 2018 (cit. on p. 6).

[33] T. Lucia, "Low frequency optimization and performance of advanced virgo seismic isolation system," Ph.D. dissertation, University of Siena, 2018 (cit. on p. 6).

[34] W. Anderson and E. Fritze, "Instrument approach system steering computer," *Proceedings of the IRE*, vol. 41, no. 2, pp. 219–228, 1953 (cit. on p. 6).

[35] R. G. Brown, "Integrated navigation systems and kalman filtering: A perspective," *Navigation*, vol. 19, no. 4, pp. 355–362, 1972 (cit. on p. 6).

[36] W. T. Higgins, "A comparison of complementary and kalman filtering," *IEEE Transactions on Aerospace and Electronic Systems*, no. 3, pp. 321–325, 1975 (cit. on p. 6).

[37] F. P. N. da Fonseca Cardoso, J. M. F. Calado, C. B. Cardeira, P. J. C. R. Oliveira, et al., "Complementary filter design with three frequency bands: Robot attitude estimation," in *2015 IEEE International Conference on Autonomous Robot Systems and Competitions*, IEEE, 2015, pp. 168–173 (cit. on pp. 6, 7, 14).

[38] S. I. Moore, A. J. Fleming, and Y. K. Yong, "Capacitive instrumentation and sensor fusion for high-bandwidth nanopositioning," *IEEE Sensors Letters*, vol. 3, no. 8, pp. 1–3, 2019 (cit. on p. 6).

[39] T.-J. Yeh, C.-Y. Su, and W.-J. Wang, "Modelling and control of a hydraulically actuated two-degree-of-freedom inertial platform," *Proceedings of the Institution of Mechanical Engineers, Part I: Journal of Systems and Control Engineering*, vol. 219, no. 6, pp. 405–417, 2005 (cit. on p. 7).

[40] D. Stoten, "Fusion of kinetic data using composite filters," *Proceedings of the Institution of Mechanical Engineers, Part I: Journal of Systems and Control Engineering*, vol. 215, no. 5, pp. 483–497, 2001 (cit. on pp. 7, 14).

[41] F. Matichard, B. Lantz, R. Mittleman, et al., "Seismic isolation of advanced ligo: Review of strategy, instrumentation and performance," *Classical and Quantum Gravity*, vol. 32, no. 18, p. 185 003, 2015 (cit. on pp. 7, 14).

[42] T. Dehaeze, M. Vermat, and C. Collette, "Complementary filters shaping using $\mathcal{H}_\infty$ synthesis," in *7th International Conference on Control, Mechatronics and Automation (ICCMA)*, 2019, pp. 459–464 (cit. on p. 7).

[43] S. Skogestad and I. Postlethwaite, *Multivariable Feedback Control: Analysis and Design - Second Edition*. John Wiley, 2007 (cit. on pp. 12, 27, 33, 34, 39).

[44] K. Furutani, M. Suzuki, and R. Kudoh, "Nanometre-cutting machine using a stewart-platform parallel mechanism," *Measurement Science and Technology*, vol. 15, no. 2, pp. 467–474, 2004 (cit. on p. 18).

[45] Z. Du, R. Shi, and W. Dong, "A piezo-actuated high-precision flexible parallel pointing mechanism: Conceptual design, development, and experiments," *IEEE Transactions on Robotics*, vol. 30, no. 1, pp. 131–137, 2014 (cit. on p. 18).

[46] J. O'Brien, J. McInroy, D. Bodtke, M. Bruch, and J. Hamann, "Lessons learned in nonlinear systems and flexible robots through experiments on a 6 legged platform," in *Proceedings of the 1998 American Control Conference. ACC (IEEE Cat. No.98CH36207)*, 1998 (cit. on p. 18).

[47] D. H. Kim, J.-Y. Kang, and K.-I. Lee, "Robust tracking control design for a 6 dof parallel manipulator," *Journal of Robotic Systems*, vol. 17, no. 10, pp. 527–547, 2000 (cit. on p. 18).

[48] H. Abbas and H. Hai, "Vibration isolation concepts for non-cubic stewart platform using modal control," in *Proceedings of 2014 11th International Bhurban Conference on Applied Sciences & Technology (IBCAST) Islamabad, Pakistan, 14th - 18th January, 2014*, Jan. 2014 (cit. on p. 18).

[49] L. Lei and W. Benli, "Multi objective robust active vibration control for flexure jointed struts of stewart platforms via $H_\infty$ and $\mu$ synthesis," *Chinese Journal of Aeronautics*, vol. 21, no. 2, pp. 125–133, 2008 (cit. on p. 18).

[50] J. Jiao, Y. Wu, K. Yu, and R. Zhao, "Dynamic modeling and experimental analyses of stewart platform with flexible hinges," *Journal of Vibration and Control*, vol. 25, no. 1, pp. 151–171, 2018 (cit. on p. 18).

[51] A. M. Rankers, "Machine dynamics in mechatronic systems: An engineering approach.," Ph.D. dissertation, University of Twente, 1998 (cit. on p. 25).

[52] A. Preumont, *Random Vibration and Spectral Analysis* (Solid Mechanics and Its Applications). Springer Netherlands, 1994 (cit. on p. 25).

[53] M. Heertjes, K. de Graaff, and J.-G. van der Toorn, "Active vibration isolation of metrology frames; a modal decoupled control design," 2005 (cit. on p. 25).

[54] J. Holterman and T. deVries, "Active damping based on decoupled collocated control," *IEEE/ASME Transactions on Mechatronics*, vol. 10, no. 2, pp. 135–145, 2005 (cit. on pp. 25, 31).

[55] G. F. Lang, "Understanding modal vectors," in *Topics in Modal Analysis & Testing, Volume 10*. Springer, 2017, ch. 8, pp. 55–68 (cit. on p. 25).

[56] S. L. Brunton and J. N. Kutz, *Data-driven science and engineering: Machine learning, dynamical systems, and control*. Cambridge University Press, 2022 (cit. on p. 27).

[57] B. Kouvaritakis, "Theory and practice of the characteristic locus design method," *Proceedings of the Institution of Electrical Engineers*, vol. 126, no. 6, p. 542, 1979 (cit. on p. 28).

[58] M. Hovd, R. D. Braatz, and S. Skogestad, "SVD controllers for $\mathcal{H}_2-$, $\mathcal{H}_\infty-$ and $\mu$-optimal control," *Automatica*, vol. 33, no. 3, pp. 433–439, 1997 (cit. on p. 29).

[59] T. Oomen, "Advanced motion control for precision mechatronics: Control, identification, and learning of complex systems," *IEEJ Journal of Industry Applications*, vol. 7, no. 2, pp. 127–140, 2018.

[60] B. J. Lurie, A. Ghavimi, F. Y. Hadaegh, and E. Mettler, "System architecture trades using bode-step control design," *Journal of Guidance, Control, and Dynamics*, vol. 25, no. 2, pp. 309–315, 2002 (cit. on p. 33).

[61] C. Collette and F. Matichard, "Vibration control of flexible structures using fusion of inertial sensors and hyper-stable actuator-sensor pairs," in *International Conference on Noise and Vibration Engineering (ISMA2014)*, 2014 (cit. on p. 35).

[62] J. E. Bibel and D. S. Malyevac, "Guidelines for the selection of weighting functions for h-infinity control," NAVAL SURFACE WARFARE CENTER DAHLGREN DIV VA, Tech. Rep., 1992 (cit. on p. 36).